**Universidade do Minho**
Escola de Medicina

Henrique Emanuel Araújo Silva

# Decoding the interplay between TAZ and metabolism in early lung development

Julho de 2019

Henrique Emanuel Araújo Silva **Decoding the interplay between TAZ and metabolism in early lung development**

UMinho | 2019

**Universidade do Minho**
Escola de Medicina

Henrique Emanuel Araújo Silva

# Decoding the interplay between TAZ and metabolism in early lung development

## Estudo da interação entre TAZ e o metabolismo no desenvolvimento pulmonar precoce

Dissertação de Mestrado
Mestrado em Ciências da Saúde

Trabalho Efetuado sob a orientação da
**Doutora Rute Carina Silva Moura**
**Doutor Marco Aurélio Gouveia Alves**

Julho de 2019

## Acknowledgments

I would like to acknowledge the School of Medicine, the School of Sciences and all the professors that accompanied me during my bachelor and master's degree. Particularly, to Doctor Rute Moura, that has been my supervisor for the last 3 years in several projects, I would like to express my profound recognition/gratitude. Thank you for believing in me and in my capability to do science, and for giving me all the support and conditions to grow as a scientist. To my supervisor Doctor Marco Alves and to Doctor Pedro Oliveira, for devoting their time and valuable experience to training me. Furthermore, I would like to acknowledge both ICVS and ICBAS teams, particularly, Hugo Silva, Pedro Silva and Ana Martins. Finally, I would like to acknowledge Professor Jorge Correia-Pinto as SSRD coordinator, my colleagues from I1.03 lab and SSRD. To all my friends that accompanied supported me thru my still short career during both bachelor and master's degrees namely, Mário, António, Bruna, Ana, Marlene, Bruna, Tiago, Miguel, Eduarda, Gonçalo, Diogo, Joana, Sara, Helena, Micaela, Andreia, Catarina, Margarida and Carlos. To my oldest friends, César, João, Carlos, Paulo, Filipa and Tiago for always believing in me and in my skills. To my family for supporting me all these years and for looking at me with proud.

Finally, and probably the most important acknowledgments, to my mother Deolinda, to my father Carlos and to my brother Carlos. Without them, my achievements would simply be impossible to accomplish. For all the sacrifices that they have done for me so that I can have a better future I can only be grateful. My success will always reflect the hard efforts that they made for me and my career. I am forever grateful and although a *thank you* seems very little considering all that you have done for me, for now is the only thing I can give you.

The work presented in this dissertation was performed at the Surgical Sciences Research Domain of the Life and Health Sciences Research Institute (ICVS), School of Medicine, University of Minho, Braga, Portugal (ICVS/3B's – PT Government Associate Laboratory, Braga/Guimarães, Portugal). The work was supported by FEDER funds, through the Competitiveness Factors Operational Programme (COMPETE), and by National funds, through the Foundation for Science and Technology (FCT), under the scope of the Project UID/Multi/50026/2019; and by the Project NORTE-01-0145-FEDER-000013, supported by the Northern Portugal Regional Operational Programme (NORTE 2020), under the Portugal 2020 Partnership Agreement, through the European Regional Development Fund (FEDER).

## Statement of integrity

I hereby declare having conducted this academic work with integrity. I confirm that I have not used plagiarism or any form of undue use of information or falsification of results along the process leading to its elaboration.

I further declare that I have fully acknowledged the Code of Ethical Conduct of the University of Minho.

## Estudo da interação entre TAZ e o metabolismo no desenvolvimento pulmonar precoce


### Resumo

A ramificação pulmonar resulta da interação entre os compartimentos epitelial e mesenquimal sendo regulada por diferentes vias de sinalização, nomeadamente, a via Hippo. A via de sinalização Hippo consiste numa cascata de cinases importante na regulação do crescimento dos órgãos, reparação e homeostasia celular. A ativação dessa via depende da fosforilação do complexo efetor YAP/TAZ. Assim, quando o complexo não está fosforilado está presente no núcleo onde se associa com fatores de transcrição, como o TEAD ou RUNX2, promovendo a transcrição de genes ligados à proliferação celular e apoptose. O impacto das vias metabólicas na regulação e atividade da via Hippo já foi descrita em alguns tecidos. No entanto, desconhece-se o impacto da modulação da via Hippo, mais concretamente da TAZ, no perfil metabólico do pulmão em desenvolvimento.

Assim, este projeto teve como objetivo estudar o impacto da modulação da TAZ no perfil metabólico do pulmão embrionário de galinha. Para tal, explantes pulmonares foram tratados, *in vitro*, com TM-25659 que promove a translocação de TAZ para o núcleo. Os pulmões tratados foram analisados morfometricamente e processados para análise por Western blot, hibridização *in situ* e qRT-PCR. Para além disso, o meio de cultura foi analisado por espectroscopia de $^{1}$H-RMN. Os explantes de pulmão tratados com TM-25659 apresentaram um aumento de 12% na ramificação, quando comparados com o controlo. Como esperado, o tratamento não afetou os níveis de expressão das proteínas YAP e TAZ, mas levou a um aumento dos níveis de expressão de *runx2*. Os resultados demonstram que a translocação de TAZ promove um aumento dos níveis de expressão de *glut8*, *mct8*, *pdh* e *ldh* quando comparados com o controlo. A análise metabolómica dos meios revelou um aumento da secreção de succinato e acetato após a estimulação da translocação de TAZ para o núcleo. Por fim caracterizou-se o perfil de metabólico do pulmão embrionário, por $^{1}$H-RMN, tendo-se detetado níveis elevados de lactato no tecido.

A manipulação do efetor TAZ nos explantes pulmonares teve um impacto discreto na ramificação pulmonar, no entanto, induziu alterações significativas nos níveis de expressão de diferentes enzimas e transportadores envolvidos no catabolismo da glicose. Além disso, alterou o perfil metabólico basal de glicolítico para oxidativo. Em conjunto, estes resultados apontam para um papel da TAZ na regulação do perfil metabólico do pulmão durante o desenvolvimento. Este estudo demonstra, pela primeira vez, a contribuição da via Hippo para a reprogramação metabólica do pulmão em desenvolvimento através da modulação da expressão de genes do catabolismo da glucose. Estes resultados podem contribuir para distinguir novos alvos terapêuticos para tratar distúrbios do desenvolvimento/doença pulmonar.



**Palavras Chave:** Desenvolvimento; Hippo; Metabolismo; Pulmão; TAZ

## Decoding the interplay between TAZ and metabolism in early lung development


### Abstract

Lung branching morphogenesis results from the crosstalk between epithelial and mesenchymal compartments and it is mainly regulated by multiple signaling pathways, namely Hippo signaling pathway. Hippo signaling pathway is a highly conserved kinase cascade that plays important roles in organ size control, repair and homeostasis. YAP and TAZ are the major transducers of Hippo pathway. The phosphorylation status of YAP/TAZ complex determines its subcellular localization and, consequently, the activation of the pathway. For instance, the non-phosphorylated YAP/TAZ is present in the nucleus where it associates with transcription factors like the TEAD family or RUNX2 promoting the transcription of target genes linked to cell proliferation and apoptosis. Several studies have described, over the years, the impact of metabolic pathways on Hippo regulation and activity. However, lung metabolic profile and the impact of Hippo modulation on the embryonic lung metabolic signature are still largely unknown.

Therefore, this project aimed to study the impact of TAZ modulation on the chick lung metabolic profile. For this purpose, *in vitro* lung explants were treated with an inducer of TAZ nuclear localization (TM-25659). Cultured lungs were morphometrically analyzed and processed for Western blot analysis, *in situ* hybridization and qRT-PCR. Moreover, culture medium was collected and analyzed by $^{1}$H-NMR spectroscopy. Lung explants stimulated with the TAZ inducer displayed an increase of 12% in branching, in a dose-dependent manner, when compared to controls. As expected, TAZ manipulation did not affect total YAP and TAZ protein expression levels but it promoted a mild increase in *runx2* expression levels. qRT-PCR analysis revealed an increase of *glut8*, *mct8*, *pdh* and *ldh* expression levels when compared to controls. $^{1}$H-NMR spectroscopy revealed an increase in the secretion of succinate and acetate to the extracellular medium after explant stimulation with a TAZ inducer. Finally, embryonic lung metabolite profile was determined, and high lactate tissue levels were detected.

TAZ manipulation had a mild impact in lung branching nonetheless it induced alterations in the expression levels of different enzymes and transporters of glucose catabolism. Furthermore, alterations in the amount of certain key metabolites was also noticed in TAZ-induced explants. Taken together, these results highlight a potential role for TAZ in the regulation of embryonic lung metabolic profile. This is the first study showing the contribution of Hippo signaling to metabolic reprograming of early lung development through the modulation of glucose catabolism-related genes. These findings may contribute to uncover new therapeutic targets to treat lung developmental disorders.



**Keywords:** Development; Hippo; Lung; Metabolism; TAZ

# Table of contents

## List of abbreviations

$^{1}$H-NMR: proton nuclear magnetic resonance

ADP: adenosine diphosphate

AEC1: alveolar epithelial cells type 1

AEC2: alveolar epithelial cells type 2

AMOT: angiomotin

AMOTL: angiomotin-like protein

AMPK: AMP-activated protein kinase

ATP: adenosine triphosphate

BCIP: 5-bromo-4-chloro-3-indoyl-phosphate

BMP: bone morphogenic protein

cDNA: complementary DNA

Dchs1: dachsous cadherin-related 1

DIG: digoxigenin

DMSO: dimethyl sulfoxide

DNA: deoxyribonucleic acid

DNase: deoxyribonuclease

ECM: extracellular matrix

EDTA: ethylenediaminetetraacetic acid

EGFR: epidermal growth factor receptor

EGTA: ethylene glycol-bis(β-aminoethyl ether)-N,N,N′,N′-tetraacetic acid

Fat4: FAT atypical cadherin 4

FGF: fibroblast growth factor

GAPDH: glyceraldehyde 3-phosphate dehydrogenase

GLUT: glucose transporter

GPCR: G protein-coupled receptor

GTP: guanosine triphosphate

HBP: hexosamine biosynthetic pathway

HEPES: 4-(2-Hydroxyethyl) piperazine-1-ethanesulfonic acid

HK: hexokinase

IMP: inosine monophosphate

JNK: c-Jun N-terminal kinase

LATS1/2: large tumor suppressors 1 and 2

LB: luria bertani

LDH: lactate dehydrogenase

LPA: lysophosphatidic acid

MABT: maleic acid buffer with Tween 20

MCT: monocarboxylate transporter

MOB1: Mps one binder 1

mRNA: messenger ribonucleic acid

MST1/2: mammalian Ste20-like kinases 1 and 2

mTOR: mechanistic target of rapamycin

mTORC1: mTOR Complex 1

mTORC2: mTOR Complex 2

*myc*: MYC Proto-Oncogene

NADH: nicotinamide adenine dinucleotide

NBT: 4-nitro tetrazolium chloride

NF2: Merlin

NTMT: alkaline phosphatase buffer

OXPHOS: oxidative phosphorylation

PBS: phosphate buffered saline

PBT: phosphate buffered saline with Tween 20

PCR: polymerase chain reaction

PDC: pyruvate dehydrogenase complex

PDH: pyruvate dehydrogenase

PI3K: phosphoinositide 3-kinase

ppm: parts per million

pYAP: phosphorylated YAP

qRT-PCR: quantitative real time polymerase chain reaction

RA: retinoic acid

RER: rough endoplasmic reticulum

RNA: ribonucleic acid

RNase: ribonuclease

rpm: rotations per minute

RUNX2: runt-related transcription factor 2

S1P: sphingosine-1-phosphate

SAV1: Salvador homolog 1

SDS-PAGE: sodium dodecyl sulfate polyacrylamide gel electrophoresis

SHH: sonic hedgehog

SRC: SRC kinase family

T3: 3,3',5-triiodothyronine

T4: 3',5',3,5 tetraiodo-L-thyronine

TAZ: transcriptional coactivator with PDZ binding motif

TBST: tris buffered saline with Tween 20

TCA: tricarboxylic acid

TEAD: TEA domain

TGF-β: transforming growth factor β

tRNA: transfer ribonucleic acid

TRs: thyroid hormone receptors

TTF-1: thyroid transcription factor-1

VEGF: vascular endothelial growth factor

VEGFR: vascular endothelial growth factor receptor

VGLL4: vestigial like family member 4

WNT: wingless-related integration site

YAP: Yes-associated protein

## Figure List

# Table List

# 1. Introduction

## 1.1. Lung development

### 1.1.1. Mammalian lung development

The lung is a complex organ that consists of two related and highly branched tubular systems, the respiratory system and the vascular system[1]. Both systems are important for the intimate contact between air and blood over a large surface area, allowing effective gas exchange[2,3]. Functionally, the respiratory system is divided into the conducting and the respiratory zone. The conducting zone consists of the proximal tubular branched system, including the trachea, and the bronchial airways. Distal bronchial airways become gradually thinner and branched, originating the respiratory bronchioles that end at the alveolar region (respiratory zone). Regarding the vascular system, this is an exceptionally branched system, completely lined by endothelial cells, thus allowing proper fulfillment of the tissue's requirements for oxygen and nutrients[4–6].

Pulmonary morphogenesis is a highly complex process that comprises several anatomical, mechanical and biochemical events commencing on the third week after conception and continuing across gestation and post-natal life until approximately 22 years of age[7]. Lung development can be divided into five different stages namely, embryonic, pseudoglandular, canalicular, saccular and alveolar, that overlap temporally and spatially[8].

The specification of the respiratory system initiates with the outward budding of the endoderm, in the anterior foregut of the respiratory diverticulum, with the expression of the transcription factor Nkx2.1, also known as thyroid transcription factor-1 (TTF-1). Evagination of the endoderm layer will generate the trachea and two lung buds emerging from the ventral side. The epithelium in the primitive buds differentiates into respiratory epithelium which underlines both proximal and distal airways[8–12].

The conducting airways are generated by an intensive and highly regulated branching process that occurs during the pseudoglandular stage. The bud tips bifurcate uninterruptedly leading to a tree-like tubular network where thin epithelial tubules are surrounded by mesenchyme derived from the mesodermal germ layer[8]. The mesenchyme at the bud tip is particularly important since cells migrate and differentiate into smooth muscle, stabilizing the cleft between the buds and facilitating branching[9–11] The crosstalk between the epithelial and mesenchymal compartments is crucial for proper lung formation and it is conveyed by several diffusible signals from multiple signaling pathways including Sonic Hedgehog

(SHH)[13], Wingless-related Integration Site (WNT)[14], Transforming Growth Factor-β (TGF-β), Bone Morphogenic Protein (BMP)[15], Fibroblast Growth Factor (FGF)[16], Retinoic Acid (RA)[17] and Hippo[18]; moreover, it involves an intense participation of extracellular matrix components such as laminin, fibronectin, syndecan, and tenascin. Altogether, they orchestrate lineage specification and expansion[10]. For instance, proximal-distal specification is governed by transcription factors such as *sox2* (proximal) *vs sox9* (distal) expression[19]. During this stage, cartilage, smooth muscle, vasculature, and mucous glands start to appear.

The alveolar differentiation that begins at the canalicular stage leads to the formation of the elementary gas exchange surface coated with cuboidal epithelium. Furthermore, at this stage, vascularization begins, the existing airways increase in size continuously, and the mesenchyme surrounding the distalmost epithelial conduits (future alveoli) becomes progressively thinner[8,9].

Afterwards, bronchial epithelial cells differentiate in alveolar epithelial cells type 1 (AEC1) and 2 (AEC2) also known as pneumocytes type 1 and 2: AEC1 are mainly involved in gas exchange whereas AEC2 are specialized in the surfactant production and can act as progenitor cells for AEC1. The decrease in interstitial tissue and reduction of airway walls, together with tissue projection into the distal airspaces, creates sac-like structures characteristic of the saccular stage[8,9]. The sacs undergo several subdivisions due to the formation of crests (septation) and cluster at the end of the branched tips. The sacs are composed by lipofibroblasts, endothelial cells, pericytes, and myofibroblasts ultimately leading to alveoli formation. Progressively, the terminal saccules increase in size and become enveloped by a bilayer of capillaries. Further epithelial differentiation and maturation of AEC2 and lamellar bodies prime the synthesis, secretion, and recycling of pulmonary surfactant[8,10].

The alveolar stage consists in the formation of alveoli by septation of the distal saccules, therefore, increasing the surface area available for gas exchange. Simultaneously, the capillary bilayer fuses into a monolayer and the microvasculature matures[8]. The air-blood barrier between alveoli and capillaries is formed and it is ultimately composed of a basement membrane and two thin layers, one of epithelium and the other of endothelium. This process continues towards the post-natal period: the organ grows, microvasculature is remodeled, and new alveoli are formed[20]. During the first years of life, alveolar size remains mostly the same, yet, during adolescence, it increases[9].

### 1.1.2. Avian lung development

The adult avian respiratory system has evident differences when compared with the mammalian adult lung: it is composed by the parabronchial lung, involved in gas exchange events, and the air sacs that are important for air movement control[21]. The primordial avian lung arises as paired evaginations

from the laryngotracheal groove after 3-4 days of development. The proximal portion of each bud will generate the extrapulmonary primary bronchus and the distal portion will give rise to the lung. Following these events, the mesobronchus, or primary bronchus, enlarges and grows towards the neighboring mesenchyme originating the secondary bronchus by lateral sprouting. This monopodial branching is morphologically comparable to the domain branching that occurs during mammalian lung morphogenesis[21,22]. At the molecular level, the avian lung also displays similarities with the mammalian lung. The signaling pathways underlying early lung organogenesis are conserved between both phyla[23–27]. Hence, despite the structural differences between mammalian and avian adult lung, the embryonic lung at early developmental stages presents molecular and morphological similarities. Moreover, the chick model (*Gallus gallus*) presents some advantages when compared to mammalian models, namely: easy surgical manipulation and a low-cost model with no need for special housing facilities that eludes progenitor death.

## 1.2. Hippo signaling pathway

Hippo signaling pathway, also known as Salvador/Warts/Hippo pathway, is an evolutionarily conserved kinase cascade, firstly discovered in *Drosophila*. Hippo core components, although conserved between species, in different contexts, tissues and even model systems present distinct functions. This pathway plays an imperative role in organ size, controlling cell number by the modulation of apoptosis and cell proliferation, as well as in cell differentiation, stem cell fate, renewal, and expansion. Furthermore, Hippo is also involved in mechanotransduction, tumorigenesis and drug resistance in mammals[12,18,28–31]. Developing organs seem to possess intrinsic signals that regulate their final dimensions[32]; for instance, Hippo regulates several aspects of lung homeostasis, repair, and development[33–36]. Hippo components comprise a series of adaptors and a core kinase cascade composed by two serine/threonine kinases, the mammalian Ste20-like kinases 1 and 2 (MST1/2) and large tumor suppressors 1 and 2 (LATS1/2); adaptor/scaffold proteins such as protein Salvador homolog 1 (SAV1) or WW5 in mammals and Mps one binder 1 (MOB1); downstream effectors, the Yes-associated protein (YAP) and its analog, the transcriptional coactivator with PDZ binding motif (TAZ) which in human present an amino acid sequence homology of approximately 45%; and finally, transcription factors like the TEAD family[12,18,37,38]. Both YAP and TAZ are emerging as key players for organ self-organization and act as the major transducers of Hippo pathway[12,30].

When Hippo signaling pathway is activated by upstream signals MST1/2 is phosphorylated and, subsequently, promotes the phosphorylation of MOB1, WW5, and LATS1/2. On its turn, LATS1/2

phosphorylates YAP/TAZ (Ser127-YAP and Ser89-TAZ, in humans) to create docking sites for the 14-3-3 proteins. Consequently, 14-3-3 proteins will bind and sequester YAP/TAZ in the cytoplasm thus inhibiting its translocation to the nucleus and promoting its proteasomal degradation. When inactivated, non-phosphorylated YAP/TAZ complex translocates into the nucleus where it associates with transcription factors, such as the TEAD family (TEAD1-4), SMADs or RUNX2, and the transcription of target genes is initiated[18,29,31,37] (Fig 1).

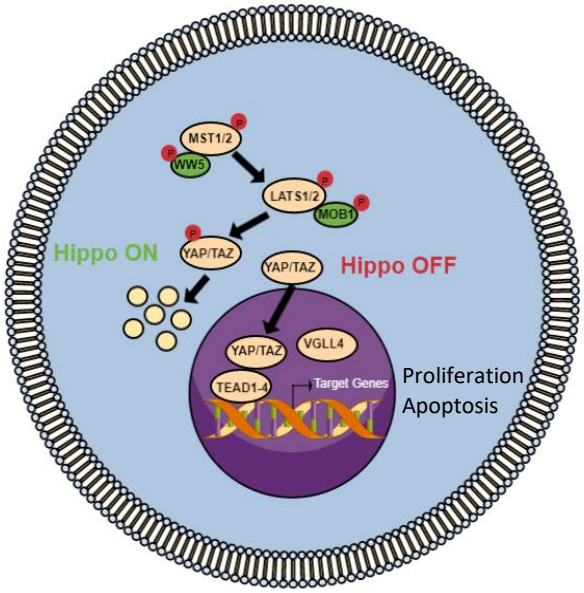


**Figure 1. Hippo signaling pathway core components.** When Hippo is active (ON), MST1/2 phosphorylates LATS1/2 that then phosphorylate YAP and TAZ; phosphorylated YAP/TAZ are targeted for degradation in the cytoplasm. When Hippo is inactive (OFF), non-phosphorylated YAP/TAZ migrate into the nucleus where compete with the VGLL4 to TEAD transcription factors binding thus, activating the transcription of specific target genes.

### 1.2.1. Hippo modulators

There are different levels of regulation for Hippo signaling cascade. Signals like increased cell-cell contact, changes on the extracellular matrix (ECM) or serum factors, repress cell proliferation and stimulate apoptosis by phosphorylating MST1/2 and, consequently, activate LATS1/2. In addition to MST1/2, mitogen-activated protein kinase kinase kinase kinase (MAP4K) and Serine/Threonine-protein kinase TAO families can also phosphorylate and, therefore, activate LATS1/2. MST1/2-promoted phosphorylation of LATS can induce LATS autophosphorylation leading to the activation of the pathway. One requirement for LATS1/2 phosphorylation, and consequently its activation, is its plasma membrane translocation assisted by NF2 protein (Merlin)[39]. Moreover, Rho GTPase transduces upstream stimuli, including GPCR signaling, mechanotransduction or the mevalonate pathway amongst others, leading to the restriction of LATS 1/2 activation[37].

On the other hand, many different stimuli can lead to YAP/TAZ cytoplasmatic retention, including regulators such as Merlin and Angiomotins (the AMOT family: tight junctions) that not only phosphorylate YAP but also promote its physical exclusion from the nucleus. The AMOT family includes AMOTL1 (angiomotin-like protein 1), AMOTL2 (angiomotin-like protein 2), and the p130 isoform of AMOT. AMOT can increase or decrease Hippo signaling depending on the family member involved[39,40]. Additionally, several other kinases have been identified and shown to phosphorylate YAP increasing its activity, including Nuclear Dbf2-related kinases 1 and 2 (NDR1 and NDR2)[41] and SRC kinases[42] (Hippo-independent YAP regulation). The AMP-activated protein kinase (AMPK), that is important in cellular energetic homeostasis, can phosphorylate YAP/TAZ leading to its inhibition by a Hippo-independent mechanism, and linking YAP/TAZ activity to cellular nutritional state[43]. Although most of the transcriptional regulation occurs via YAP/TAZ phosphorylation, recent studies unveiled the fact that phosphorylation of TEAD via p38 Mitogen-Activated Protein Kinase (MAPK) promotes cytoplasmatic localization and consequently reduces the transcriptional activity of the YAP–TEAD complex[4]. Phosphorylation of Ser311-TAZ and Ser381-YAP mediated by LATS1/2, primes the subsequent phosphorylation by Casein kinase 1 isoform delta/epsilon; afterwards, the recruitment of E3 ubiquitin ligase leads to ubiquitination and proteasomal degradation of YAP/TAZ[12].

Additionally, YAP/TAZ nuclear translocation is under the control of cellular polarity and shape, which is regulated by the cytoskeleton. The cytoskeleton is responsible for physical inputs that guide YAP/TAZ into specific gene expression patterns that mostly depend on the context of biological responses[44]. Furthermore, cellular structural characteristics must be linked to cellular metabolism and other environmental inputs like, for instance, morphogens or nutrient accessibility. The synchronization between cell behavior and surrounding mechanical cues which is translated into signaling paths and affects gene expression is called mechanotransduction. YAP/TAZ promotes the transcription of genes that promote F-actin remodeling and mechanical signaling that will regulate YAP/TAZ activity[45,46].

Several other mechanisms of regulation direct the activity of Hippo including: protocadherins Dachsous and Fat (Dachsous-Fat system), expressed in opposing gradients in response to morphogens, that regulate Hippo and planar cell polarity; cell polarity with the participation of mammalian components of tight or adherens junctions complexes; cell density; integrin signaling and ECM attachment; and mechanical stress (mechanical force) at adherens junctions, focal adhesions, and cytoskeletal tension[12,29]. In figure 2 are summarized all the factors that influence the activity of Hippo.

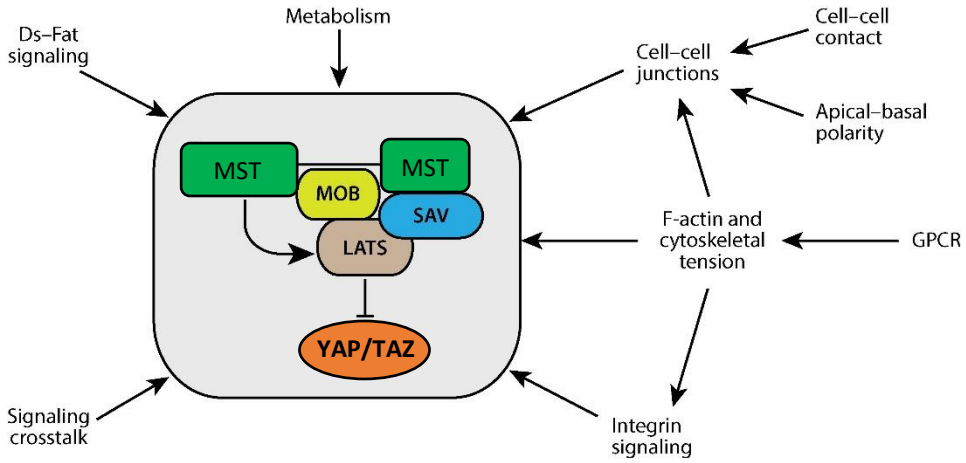


**Figure 2. Hippo signaling pathway activity regulation.** Factors that influence the activation of Hippo pathway kinases and YAP/TAZ. Upstream cues include Ds–Fat signaling; crosstalk from other major signaling pathways including EGFR, WNT, BMP, SHH, and GPCR; integrin signaling; cellular metabolism; metabolic pathways; F-actin levels, tension in the cytoskeleton, and mechanical stress at cell junctions and focal adhesions. Adapted from[29].

### 1.2.2. Hippo targets and effectors

Hippo response is conveyed by YAP and TAZ proteins, however, the association with transcription factors is imperative since YAP and TAZ do not possess DNA binding domains. The TEAD family and SMADs family of transcription factors associate with YAP/TAZ; moreover, other transcriptional factors such as β-catenin[47] or the runt-related transcription factor 2 (RUNX2)[48] may be also recruited depending on the context. Concerning TEAD proteins, in vertebrates, they can be associated with the vestigial like family member 4 (VGLL4), a cofactor of TEAD, which competes with YAP/TAZ for TEADs binding, thus repressing its action (Fig 1)[49].

The most studied biological function dependent on YAP/TAZ is cell proliferation. The expression of cell cycle regulators induced by YAP/TAZ controls this process, amongst them: cell cycle genes including DNA repair and replication machinery, cyclins and mitotic-related proteins. Particularly, *cyce* and *e2f1,* growth-promoting genes like *myc* and inhibitors of apoptosis such as *birc3* and *diap1* stand out as Hippo target genes[50]. Additionally, genes like *ctgf*, *cyr61*, *axl*, *birc5*, *areg*, and *ankrd1* can also be targets of Hippo effectors. Moreover, the expression of anti-apoptotic genes such as the inhibitor of apoptosis protein (IAP) and *bcl2* families is also controlled by YAP/TAZ and results in cell resistance against apoptosis[12,29,45]. On a metabolic point of view, mTOR signaling is activated by YAP/TAZ. The transcription of several regulators of this pathway is on the basis of this transcriptional program[51]. Additionally, the transcriptional regulation of enzymes involved in glycolysis, glutamine metabolism, nucleotide synthesis, and Hexosamine Biosynthetic Pathway (HBP) can also regulate YAP/TAZ activity[45].

### 1.2.3. Hippo functions

Hippo was initially recognized as a regulator of organ size due to its control over cell proliferation and, later, as a sensor of cell density[52,53]. Nonetheless, organ size regulation does not occur in the same way in different types of vertebrate organs. It has already been described that YAP promotes overgrowth in organs like the liver[54] but not, for instance, in the kidney[55]. In addition, YAP/TAZ activation (Hippo off) promotes cell proliferation at low cell density whereas strong Hippo signaling (Hippo on) suppresses cell proliferation at high cell density leading to contact inhibition (cell junctions and polarity appearance). Moreover, ligands from other signaling pathways like Epidermal Growth Factor Receptor (EGFR) or WNT also promote growth and are linked to YAP since these ligands are transcriptional targets of YAP and/or TAZ[29,53].

YAP/TAZ are deeply linked with cell fate decisions in many aspects of development. In early mouse embryogenesis, YAP/TAZ complex is involved in the division of the blastocyst into the inner cell mass (ICM) and trophoectoderm (TE)[56]. Hippo signaling is activated on the inner cells that will generate the ICM; on the other hand, in blastocyst cells, Hippo is downregulated leading to YAP/TAZ activation thus promoting the formation of TE. This regulation seems to be due to AMOT that promote LATS activation, and to cell stretching that activates YAP/TAZ in TE cells[57,58].

In recent years, many studies point to the fact that YAP/TAZ complex is essential for progenitor or stem cell fates in many mammalian tissues including muscle, skin, liver, nervous system, teeth, pancreas, mammary gland and in the lung[59]. YAP/TAZ promotes survival of human embryonic stem cells, suppresses differentiation and can convert differentiated cells into stem cells. Furthermore, YAP/TAZ are involved in mesenchymal stem cell differentiation in culture conditions[60,61].

Regarding cell behavior, YAP/TAZ have very important roles on vasculature since they act as downstream effectors of Vascular Endothelial Growth Factor (VEGF) and Vascular Endothelial Growth Factor Receptor 2 (VEGFR2) signaling[62]. VEGF activates YAP/TAZ thus promoting the transcription of genes involved on angiogenesis[62,63]; consequently, when dysregulated it can cause several diseases like pulmonary hypertension or atherosclerosis[64]. Hippo is important for the proper functioning of the immune system mostly due to the control of LATS activity in tumors[65].

Considering the role of YAP/TAZ in regulating progenitor cell fate and organ growth, it is not surprising that it is involved in tissue repair and regeneration, and wound healing. In fact, alterations in cell density, cell-cell contact, and cell stretching after tissue damage, wound, inflammation or infection,

and corresponding signaling pathways can activate YAP/TAZ. YAP/TAZ have key roles in the regeneration of several mammalian tissues like skin, mammary gland, intestine, and lungs[66].

Hippo dysregulation is associated with many diseases. For instance, in pulmonary fibrosis, the activation of YAP/TAZ can promote abnormal and excessive ECM deposition by activated fibroblasts leading to cellular dysfunction and tissue stiffening[67,68]. Moreover, many types of cancers including colon, breast, ovarian, pancreatic, liver, skin, brain and lung show high levels and increased nuclear localization of YAP/TAZ. Besides, high levels of YAP/TAZ are generally associated with poor prognosis in many human cancers. Not only YAP/TAZ overactivation is associated with cancer but also mutations in the upstream Hippo signaling modulators like EGFR-RAS, c-Jun N-terminal kinases (JNK), SRC, G protein-coupled receptors (GPCR), WNT or phosphoinositide 3-kinase (PI3K) signaling pathways. In addition to the impact in cell proliferation, there are other effects associated with YAP/TAZ-related oncogenesis like cancer stem cell behavior support, alterations on metabolism and metastasis promotion, particularly TAZ[69].

### 1.2.4. Hippo and crosstalk with other signaling pathways

Hippo signaling is a major regulator of cell fate and tissue growth, however, it does not act alone, and it depends on the crosstalk with other signaling pathways. For instance, signaling pathways with GPCRs can influence the activity of Rho which, by its turn, can regulate YAP and TAZ[70]. Many hormones, growth factors or metabolic regulators can act through different classes of GPCRs that can either induce or repress YAP/TAZ activity[71,72]. For instance, lysophosphatidic acid (LPA) and sphingosine-1-phosphate (S1P) inhibit LATS1/2 and activate YAP/TAZ[70]. In addition to LPA and S1P, estrogens, thrombin, and acetylcholine can activate YAP/TAZ. On the other hand, GPCR signaling caused by epinephrine or glucagon can repress YAP/TAZ activity[70,71,73,74].

YAP/TAZ complex is a transcriptional mediator of WNT signaling. The destruction complex that controls the intracellular amount of β-catenin also regulates YAP/TAZ activity. Cytoplasmatic YAP/TAZ facilitates the formation of the destruction complex thus promoting β-catenin degradation. Likewise, YAP/TAZ translocation into the nucleus can lead to β-catenin nuclear localization. Taken together, it appears that activation of Hippo antagonizes the WNT-β-catenin signaling. Additionally, YAP/TAZ can inhibit Dishevelled, a downstream signaling mediator, and, therefore, inhibit WNT signaling[47]

Some reports have shown a crosstalk between TGF-β and YAP/TAZ. The Hippo effectors are important in determining the action of the SMAD2/3-SMAD4 complex that participates in pluripotency maintenance as well as in mesodermal differentiation during the onset of gastrulation and mesodermal specification. The crosstalk between these two signaling pathways has been observed during lung

development[12,75]. Hippo is also related to the BMP pathway since YAP/TAZ can interact with the SMADs. Furthermore, EGFR, JNK, and SHH can interact with YAP/TAZ and regulate its activity[50].

Additionally, Hippo effectors YAP/TAZ interact with Notch signaling. The regulation of Notch ligands promoted by YAP/TAZ in a single cell causes the activation of Notch signaling in the surrounding cells. In fact, many Notch ligands are translated in a YAP/TAZ-induced manner and regulate many processes during development including differentiation of neural crest progenitors during arterial wall development or the somatic segmentation clock[76,77].

During vascular development, the effect on endothelial cells promoted by VEGF signaling promotes YAP/TAZ activation that, due to its translational program, leads to a proper VEGF receptor trafficking[62,78].

### 1.2.5. Hippo signaling and metabolism

Signaling pathways and metabolism cooperate to allow proper tissue growth and homeostasis. Insulin/Insulin-like growth factor signaling can activate YAP/TAZ and promote tissue growth, through the action of phosphoinositide-dependent kinase 1 (PDK1) and Protein kinase B, also known as AKT[80]. The decrease in glucose levels leads to AMPK activation and, by its turn, this cellular energy sensor decrease YAP/TAZ activity both directly phosphorylating YAP and phosphorylating AMOTL1 to promote LATS activation[43,79,81]. Recently, it was described that glucose availability can sustain YAP activity through the hexosamine biosynthesis pathway and its impact on the *O*-GlcNAc transferases that attach a GlcNAc group to Thr or Ser residues. High glucose levels promote the formation of uridine diphosphate *N*-acetylglucosamine (UDP-GlcNAc) which increases YAP *O*-GlcNAcylation, stabilizing YAP protein and decreasing its phosphorylation by LATS[72,74,82]. Furthermore, the glycolysis rate-limiting enzyme phosphofructokinase 1 (PFK1) can bind directly to TEAD stabilizing the interaction with YAP/TAZ and, consequently, enhancing YAP/TAZ activity by the formation of the nuclear complex PFK1-YAP/TAZ-TEAD. On the other hand, YAP induces the transcription of genes involved in the hexosamine biosynthesis pathways which promote *O*-GlcNAcylation and increase the glucose uptake[83].

Cell size and proliferation are deeply responsive to nutrients and growth factors availability, as well as cellular energy levels, mainly via TOR signaling. The mTORC1 kinase complex supports YAP/TAZ activity by the inhibition of the autophagosome-dependent lysosomal degradation in a model of perivascular epithelioid tumors[51]. mTORC2 kinase complex can activate YAP/TAZ through the inhibitory phosphorylation of AMOT proteins or MST1[84,85]. On the other hand, the tuberous sclerosis protein (TSC)-Tor pathway can influence both levels and activity of YAP and TAZ[51]. Moreover, aerobic glycolysis regulates

YAP activity, promoting an increased glucose uptake[82,83]. Furthermore, YAP activation leads to TOR signaling activation[86].

Gluconeogenesis is regulated by insulin and glucagon and involves the activity of many transcription factors[87]. Glucagon stimulates gluconeogenesis by activation of protein kinase A (PKA) that, in a cAMP-dependent manner, promotes the activation of several transcription factors culminating in the expression of gluconeogenesis-related genes[88]. Recently it was reported that high levels of glucagon inhibit both expression and activity of YAP and TAZ. After binding to a GPCR, glucagon promotes the accumulation of cAMP. Consequently, that leads to PKA activation thus inhibiting Rho GTPase; LATS1/2 is phosphorylated leading to YAP/TAZ cytoplasmatic retention and degradation[70,89]. Several recent lines of evidence have shown that YAP suppresses gluconeogenesis by suppressing or decreasing the expression of gluconeogenesis-related genes[90].

Cell proliferation and migration are influenced by lipid metabolism. The mevalonate/cholesterol biosynthetic pathway can regulate YAP/TAZ activity. This pathway uses acetyl coenzyme A to synthesize steroids and nonsteroidal lipids. Some metabolic intermediaries such as farnesyl pyrophosphate (FPP) and geranylgeranyl pyrophosphate (GGPP) are involved in protein prenylation contributing to the maintenance of cell and lipid metabolism. Mevalonic acid sustains YAP/TAZ activity due to the production of GGPP which is attached to the RhoA-GTPase. Membrane active RhoA can activate YAP/TAZ in a LATS1/2-independent manner[91,92]. In addition to enzymes, free fatty acids can as well regulate YAP/TAZ activity, for instance, palmitate is able to promote YAP transcriptional activity in pancreatic β-cells in an F-actin-dependent manner; additionally, it is involved in a post-transcriptional modification of TEAD, S-palmitoylation, therefore indirectly regulating YAP/TAZ transcription since it stabilizes YAP/TAZ binding to TEAD[93,94].

Cells obtain most of the energy and some biosynthetic precursors by the tricarboxylic acid (TCA) cycle. Glutaminolysis is the metabolic pathway responsible for the conversion of glutamine into glutamate and ammonia by the action of glutaminase. Then, glutamate dehydrogenase and transaminases convert glutamate into α-ketoglutarate that can supply the TCA cycle, hence, contributing to ATP production. Besides ATP, this pathway supplies nitrogen and carbons for protein, nucleotide and lipid synthesis[95,96]. It has been recently described that YAP/TAZ activation promotes an increase in glutamine levels, promotes nucleotide synthesis and induces expression and activity of glutamine synthetase[97]. In endothelial cells it was observed that YAP/TAZ knockdown reduces lactate production (decrease the extracellular

lactate/pyruvate ratio) however when YAP/TAZ expression is stable, extracellular lactate, glutamate and aspartate levels increase whereas glutamine decrease[98].

## 1.3. Hippo signaling during lung development

In recent years, the role of Hippo signaling and, particularly, of YAP and TAZ have been explored at the developmental level. YAP-deficient embryos show premature lethality mostly due to failures on chorioallantoic attachment and in yolk sac vasculogenesis[99]. TAZ null homozygote embryos show high perinatal lethality in four-fifths of the cases and present renal and pulmonary defects[100,101]. Moreover, double knockout embryos for YAP and TAZ die before the morula stage. Taking this into consideration, YAP and TAZ present some redundant functions but, in fact, play slightly different biological roles[56].

*taz* knockout mice display major defects in alveolarization and the formation of renal cysts. The adult animals display brutally enlarged lung air spaces that resemble human pulmonary emphysema[100,101]. Moreover, TAZ interacts and activates TTF1, a transcription factor very important during branching morphogenesis and the development of lung and thyroid. However, the expression levels of TTF1 remain constant in *taz* knockout lungs[101].

More recently, YAP was shown to play crucial roles in the regulation of cell differentiation in both embryonic and adult lung cells. YAP is responsible for marking the limit between progenitors that will then generate the airways *vs* alveoli. In the airways, YAP is phosphorylated and therefore retained in the cytoplasm (Hippo on); in the alveoli, YAP is unphosphorylated and localized in the nucleus (Hippo off). Epithelial progenitor cells are the major contributors for proper lung branching morphogenesis. They initially determine the proximal-distal patterning and, later, the morphology and cellular types of the developing organ. In mouse, this type of patterning is governed by two transcription factors: SOX2 and SOX9. SOX2 is localized on the proximal epithelial and SOX9 in the distal epithelium where new branches appear. The distribution of these two transcription factors leads to proper cell proliferation and differentiation and, therefore, promotes correct lung branching[102]. YAP regulates *sox2* expression and sensitize cells to TGF-β signaling[35]. Moreover, adult basal stem cells are significantly decreased due to uncontrolled differentiation in the absence of YAP. On the other hand, when YAP is overexpressed in the same cells, stem cell proliferation is promoted thus resulting in epithelial hyperplasia and stratification[34].

Other Hippo components are involved in lung organogenesis. Absence of Dchs1 and Fat4 in mice causes a reduction in lung size, whilst other organs are not significantly decreased[103]. Furthermore, *mst1/2* conditional knockout from respiratory epithelium promotes profound alterations in the lung,

namely, reduced surfactant proteins, impaired peripheral lung differentiation and maturation leading to perinatal lethality[36,104].

Unpublished results from our laboratory have shown by, *in situ* hybridization, that the molecular machinery of Hippo signaling is present throughout the early stages of chick lung branching, except for *mst2* and *lats2*. For instance, *taz* mRNA expression was detected exclusively in the pulmonary epithelium of the main bronchi accompanying the appearance of new branches. Moreover, *in vitro* lung explants treated with verteporfin, a compound that prevents YAP/TAZ-TEAD association impairing the specific gene expression profile, displayed a reduction in size and branching when compared to the control. Overall, this study demonstrated the presence of Hippo signaling in early stages of avian pulmonary branching and that Hippo is active and possibly involved in lung growth control.

## 1.4. Metabolism during development

Metabolism is on the basis of cellular activity and it is responsible for both energetic and metabolic intermediaries needed to properly sustain proliferating cells and growing tissues. Glucose catabolism, particularly, glucose aerobic oxidation is the main source of energy for normal cells[105] Glycolytic reactions occur in the cytosol and convert glucose into pyruvate[106]. Only 5% of the chemical energy of glucose is released during glycolysis, which indicates that 95% of energy prevail in the two resulting pyruvate molecules. Pyruvate can serve many destinations, among them to serve as a substrate for acetyl-CoA production, to be used in alanine synthesis or to be diverted for lactate production[107].

During development, cells are actively proliferative. Metabolism of proliferating cells needs to be fine-tuned to meet their high energy demands and facilitate the uptake and incorporation of nutrients required to sustain growth. Hence, glycolytic metabolism is suggested to be the primary energy source for embryo and lung development. Despite the low energetic yield of glycolysis (2 molecules of ATP per molecule of glucose), this process is faster than oxidative phosphorylation, produces metabolites with reducing power (such as NADH) and metabolic intermediaries that fuel anabolic pathways, thus supporting tissue growth. Consequently, intensive glucose metabolism is expected to fulfill these requirements[108].

Bulusu *et al.*[109] found that during mouse embryo presomitic mesoderm (PSM) development there is a gradient of glycolytic activity that is more evident in the posterior undifferentiated PSM. This study states the existence of aerobic glycolysis during mouse organogenesis and that pyruvate acts as a biosensor that indirectly mirrors glycolytic activity. A different study described a glycolytic gradient in the mouse tailbud and in developing chicken embryos. Moreover, the crosstalk between metabolic regulation

and signaling, namely FGF and WNT was also observed. Finally, it was shown that glycolysis regulates cell motility, body axis elongation, and extracellular pH[110]. Overall, these results confirm that gradient glycolytic activity is conserved in both models. Moreover, unpublished results from our laboratory have shown that during early lung branching morphogenesis, the pulmonary metabolic preference lays on a glycolytic-lactate based profile. In fact, branching morphogenesis is accompanied by an increase in lactate and acetate production.

Nevertheless, the relationship between TAZ and metabolism, in the developing lung is still unknown. The disclosure and characterization of this association, during lung branching morphogenesis, is of great importance to reveal novel therapeutic approaches that may contribute to treating lung disorders.

# 2. Aims

The metabolic activity is crucial to maintaining cell homeostasis and, unsurprisingly, it is highly controlled by several signaling pathways and growth factors. During lung development there is an intense crosstalk between different compartments and signaling pathways, among them Hippo. Hippo signaling regulates cellular events associated with tissue growth and maintenance, thus influencing organogenesis. To sustain this process, cells and tissues need energy supply and metabolic intermediaries. In this sense, it is imperative to understand the relationship between Hippo signaling, metabolism and lung development. In this work we hypothesized that Hippo signaling, namely its effector TAZ, might be regulating metabolism during early stages of chick lung development. Therefore, the main purpose of this project was to characterize the role of Hippo signaling on metabolic pathways associated with embryonic lung development.

This work aimed to accomplish the following specific objectives:

- Determine the role of TAZ in early chick lung development, using an *in vitro* lung explant system

- Characterize TAZ-induced lung metabolic profile, by $^{1}$H-NMR spectroscopy

- Assess the expression levels of key metabolic enzymes and transporters in TAZ-induced metabolism, by qRT-PCR

- Characterize the normal embryonic chick lung metabolome, by $^{1}$H-NMR spectroscopy

# 3. Materials and Methods

## 3.1. Ethical statement

The work performed during this master thesis was carried out in the chick model (*Gallus gallus*), at early stages of development. The use of fertilized chicken eggs does not require ethical approval from the review board institution or the ethical committee, which is in accordance with the Directive 2010/63/EU of the European Parliament and of the Council of 22 September 2010 on the protection of animals used for scientific purposes. The Portuguese Directive 113/2013 of 7 August 2013 does not contain any kind of restriction to the use of non-mammalian embryos.

## 3.2. Tissue harvesting

Fertilized chicken eggs were obtained from commercial sources and incubated (Termaks KB400, Norway) during a period of approximately 5 days at 37°C, and with 49% of humidity. Embryonic chick lungs were dissected in PBS 1x (Phosphate Buffered Saline) using a dissection microscope (Olympus SZX16, Japan). Then, lungs were classified in stage b1, b2 and b3 according to the number of secondary buds formed: 1, 2 or 3 per bronchus, respectively[23]. For *in vitro* explant culture, dissected lungs were used immediately to proceed with culture (section 3.3). For protein, RNA and metabolome analysis, whole lungs or lung explants were collected on ice, assembled in pools, snapped frozen in liquid nitrogen and stored at -80˚C until further use (section 3.5, 3.8, and 3.9, respectively). For *in situ* hybridization, whole lungs or lung explants were fixed in a 4% formaldehyde solution (2 mM EGTA in PBS pH 7.5), and stored at 4°C, overnight. Subsequently, tissues were dehydrated in PBT (PBS 1x with 0.1% Tween 20) with increasing concentrations of methanol and stored at -20°C (section 3.7).

## 3.3. Lung explant culture

Lung branching morphogenesis depends on intensive crosstalk between epithelium and the surrounding mesenchyme. *In vitro* embryonic lung explant culture is a very useful technique to study the interactions between epithelial and mesenchymal compartments, in the absence of maternal influence or blood flow. With this approach, morphogenesis can be manipulated by altering a chemically defined culture media to perform, for instance, loss or gain of function studies and assess the role of particular growth factors and signaling pathways in pulmonary branching[111,112]. Lung explants may grow *ex vivo* in an air-liquid interface for time periods between 12 and 96 hours thereby permitting the evaluation of whole

organ growth over time. Moreover, with this methodology, it is possible to evaluate the components of the culture medium and assess, for instance, which metabolites are being consumed or secreted[112].

Firstly, Nucleopore polycarbonate membranes with an 8 µm pore size (Whatman, USA) were presoaked in 400 µL of Medium 199 (Sigma, USA) for one hour, at room temperature, in a 24-well culture plate (SPL Life Sciences, Korea). Next, Medium 199 was substituted by 200 µL of Medium 199 supplemented with 5% heat-inactivated fetal calf serum (Invitrogen, USA), 10% chicken serum (Invitrogen), 1% L-glutamine (Invitrogen), 1% penicillin 5000 IU/mL, streptomycin 5000 IU/mL (Invitrogen) and 0.25 mg/mL ascorbic acid (Sigma).

Subsequently, stage b2 lungs were placed on top of the membranes and incubated in a 5% $CO_2$ incubator at 37°C, for 30 minutes. After that period, floating cultures were photographed, and the stage confirmed. Next, explants were randomly assigned to one of five experimental groups: DMSO (0.1%) or TM-25659 (5 µM, 10 µM, 15 µM, and 20 µM). TM-25659 was selected because it enhances the translocation of TAZ to the nucleus. Since TM-25659 must be dissolved in DMSO, control explants were supplemented with this solvent. Explants were incubated for 48h and the culture medium, supplemented accordingly, replaced after 24h. Branching morphogenesis was monitored, by photographing the explants, every 24h: at D0 (0h), D1 (24h) and D2 (48h) of culture[24]. At D2, lung explants were washed three times with filtered PBS 1x, snap-frozen and stored at -80˚C for further processing for protein, RNA or metabolite extraction; for *in situ* hybridization, explants were fixed and processed as previously described (section 3.2). Culture medium was collected at D0, D1, and D2, and kept at -20˚C for metabolite analysis (section 3.9.1)[23].

## 3.4. Morphometric analysis

To determine the impact of TM-25659 on lung organogenesis, D0 and D2 lung explants were morphometrically analyzed. The total number of peripheral airway buds was determined at both time points (n≥15/condition). Additionally, the internal perimeter of the lung (epithelium) and the outer perimeter of the lung (mesenchyme) were assessed at D0 and D2 (n≥15/condition) using Axion-Vision Rel. 4.3 (Carl Zeiss GmbH, Germany). With these measurements, the area and perimeter of both compartments can be calculated. The results of branching and morphometric analysis were expressed as D2/D0 ratio[27]. All quantitative morphometric data are presented as mean ± SEM with a statistically significant level of 5% ($p<0.05$). Statistical analysis was performed using GraphPad Prism 6 (USA). Normality of distribution and homogeneity of group variances were tested, and One-Way ANOVA was performed.

## 3.5. Protein extraction and quantification

### 3.5.1. Total protein extraction

Pooled samples of lung explants (3 pools/condition: 10 lungs/pool) were homogenized in a small volume of a specific lysis buffer containing: HEPES, pH 7.5, 20 mM; Glycerophosphate, 50 mM; EGTA, 2 mM; Sodium Vanadate, 1 mM; 10% Glycerol; 1% Triton X-100; 1% complete protease inhibitor cocktail (Sigma). Tissues were mechanically homogenized on ice using a pellet pestle cordless motor (Kontes Glass, USA), during 3 cycles of 10 seconds at maximum speed, followed by 2 minutes on ice. The homogenate was centrifuged at 13000 rpm for 30 minutes, at 4°C, the supernatant was collected and stored at -80°C.

### 3.5.2. Protein quantification

Protein quantification was performed by the Bradford assay. The Bradford method is a rapid, sensitive, reproducible and low interference protein quantification method that uses Coomassie Brilliant Blue G-250. This dye reacts with basic amino acid residues in the proteins changing the absorption maximum from 465 to 595 nm[113,114]. Coomassie Brilliant Blue G-250 changes from red to blue form when binding between protein and dye occurs[113]. The Bradford calibration curve was generated using standard solutions with different Bovine Serum Albumin concentrations ranging from 0.1 to 0.7 μg/μl. The spectrophotometric readings were made in duplicate and linear regression applied to obtain the standard curve. The different samples were read in duplicate, and the concentration of total protein determined by the linear regression equation.

## 3.6. Western blot

Western blot is a widely used technique that allows the identification of specific proteins from a complex mixture (homogenate) extracted from cells or tissues. Briefly, proteins are separated by size thru gel electrophoresis, in denaturing conditions, and then transferred to a membrane. Subsequently, the membrane is incubated with a primary antibody against the protein of interest that is then recognized by a secondary antibody coupled to an enzyme. Finally, in the presence of proper substrates, the enzymatic reaction occurs, and the product is detected by an imaging system[115]. This immunodetection technique enables the quantification of proteins with different expression levels in the same blot. Additionally, a normalization method based on housekeeping proteins, such as β-tubulin, is required and essential as a loading control[116].

### 3.6.1. SDS-PAGE

Sodium dodecyl sulfate polyacrylamide gel electrophoresis (SDS-PAGE) constitutes the most common way of separating a complex mixture of proteins. SDS is a denaturing anionic detergent that disturbs native protein conformation by breaking non-covalent bonds and gives a uniform net negative charge to the protein molecules. When exposed to an electrical field, proteins migrate to the positive electrode and separate only according to their molecular weight[117,118]. Samples were prepared with a commercial Laemmli buffer (Bio-Rad, USA) mixed with β-mercaptoethanol (Sigma) to guarantee the reduction of disulfide bridges.

Ten μg of total protein were loaded onto 10% acrylamide minigels and electrophoresed at 100 V, for approximately 2 hours, in the vertical Mini-PROTEAN Tetra Cell (Bio-Rad). 10% resolving gels were prepared with: 10% Acrylamide/Bis-acrylamide (Bio-Rad); 0.375 M Tris-HCl, pH 8.8; 0.1% Sodium Dodecyl Sulfate (SDS). Finally, 0.05% Ammonium Persulfate (APS) and 0.014% Tetramethylethylenediamine (TEMED) were added to accelerate polymerization. The 4% stacking gel was prepared with: 4% Acrylamide/Bis-acrylamide; 0.126 M Tris-HCl, pH 6.8; 0.1% SDS. Finally, 0.05% of APS and 0.008% TEMED were added.

Afterwards, the polyacrylamide gel was transferred to 0.2 μm nitrocellulose membrane (Trans-Blot Turbo RTA Mini Nitrocellulose Transfer Kit, Bio-Rad) in the Trans-Blot Turbo Transfer System (Bio-Rad) for 7 minutes, at 2 amperes and 25 volts. After transfer, membranes were incubated with Ponceau S [(0.1% Ponceau S (w/v) in 5% acetic acid)] to confirm protein transfer.

Membranes were then blocked, for 2 hours at room temperature, with a blocking buffer [5% BSA in TBST (20 mM Tris, 0.137 M NaCl, 0.1% Tween, pH 7.6)]; after washing with TBST, blots were incubated with primary antibodies diluted in 5% BSA in TBST, overnight at 4°C. The antibody dilution was settled to 1:2000 for YAP/TAZ (#ab8418, Rabbit mAb, Cell Signaling Technology, USA). For loading control, blots were probed with β-tubulin (1:200000; #ab6046, Abcam Inc., UK). Membranes were then washed in TBST, and next incubated with anti-rabbit secondary horseradish peroxidase-conjugated antibody (1:2000; #7074, Cell Signaling Technology Inc.) in 2% skimmed milk in TBST, according to the manufacturer's instructions. Finally, and after washing with TBST, membranes were developed with Clarity Western ECL substrate (Bio-Rad) and the chemiluminescent signal was captured using the Chemidoc XRS (Bio-Rad). Quantitative analysis was performed with ImageLab software (Bio-Rad).

Three independent experiments were performed, and each sample was run in triplicate. For loading control, β-tubulin was used. Semi-quantitative expression analysis of total YAP and total TAZ was

performed using an Image Analysis Software (Bio-Rad, USA). All quantitative data are presented as mean ± SEM with a statistically significant level of 5% ($p<0.05$). Statistical analysis was performed using GraphPad Prism 6 (USA). Normality of distribution and homogeneity of group variances were tested, and One-Way ANOVA was performed.

## 3.7. Whole-mount *in situ* hybridization

*In situ* hybridization is a semi-quantitative technique that allows the detection of specific mRNA in the tissue thus revealing its spatial localization in the different cellular compartments. It requires the use of single-strand antisense RNA probes that are reverse and complementary to the mRNA to be detected. In the appropriate conditions, the labeled RNA probe recognizes and binds to the target mRNA, producing a stable hybrid. This hybrid is then detected through the use of an antibody that recognizes the specific labeling followed by an enzymatic reaction that produces a chromogenic precipitate. The presence of this precipitate reveals to the expression site of the mRNA[119,120]. The antisense probe used in this work, *runx2*, was already described in the literature and the plasmid was kindly provided, in filter paper, by the authors[121].

### 3.7.1. Probe preparation

The *runx2* plasmid was eluted using ultrapure water and left at room temperature, for 2 hours. Next, the plasmid was transformed by heat shock protocol using competent of *Escherichia coli* (XL1-blue) cells[122]. Cells were plated in Luria broth (LB) agar plates (0.5% yeast extract, 1% NaCl, 1% tryptone, 2% agar) supplemented 1 µg/mL ampicillin (NZYTech, Portugal), and kept overnight at 37°C.

Subsequently, selected isolated colonies were inoculated in LB liquid medium, overnight, and plasmid DNA was extracted using GeneJET Plasmid Miniprep Kit (Thermo Fisher Scientific, USA), according to the manufacturer's instructions. Finally, plasmid DNA concentration was determined by NanoDrop spectrophotometer (NanoDrop ND-1000, USA) and sample purity was estimated based on the 260/280 ratio.

### 3.7.2. Probe synthesis

The fragment of interest, containing *runx2* sequence, was obtained by PCR amplification (NZYTaq 2x Green Master Mix; NZYTech) using M13 universal primers and a standard protocol. To confirm the presence of the expected band, a 0.8% agarose gel was used. The PCR reaction was cleaned using GRS PCR & Gel Band Purification Kit (Grisp, Portugal). RNA antisense probes were obtained through an *in vitro* transcription reaction using approximately 750 ng of the purified fragment as a template. For the *in vitro*

transcription reaction, SP6 RNA polymerase and a nucleotide mix containing uracil bound to Digoxigenin (DIG) were used (Roche Applied Sciences, USA). DIG is the key for the detection procedure since it is recognized by an anti-DIG antibody coupled to an enzyme (alkaline phosphatase) that, in the presence of specific substrates, produces a blue precipitate.

### 3.7.3. *In situ* hybridization

*In situ* hybridization procedure was performed according to Henrique *et al.* protocol with minor modifications[123]. Whole lungs (6 lungs/stage) or lung explants (5 lungs/condition) and 2 control embryos stage HH25 were rehydrated through a series of methanol into PBT at room temperature. After rehydration, both lungs and embryos were washed twice with PBT and treated with proteinase K, 20 mg/mL, in PBT, for 2 and 35 minutes respectively, at room temperature. This serine protease permeabilizes tissues to facilitate the entry of the RNA probes. Subsequently, tissues were washed twice in PBT to remove completely the proteinase K and treated with a fixing solution (formaldehyde 3.7%; glutaraldehyde 0.1M in PBT) for 20 minutes. Then, tissues were washed with PBT and hybridization solution [formamide 50%; saline-sodium citrate (SSC), 1.3x, pH 5; EDTA, 0.005M, pH 8; t-RNA, 50 mg/mL; Tween 20, 0.2%; 3-[(3-Cholamidopropyl) dimethylammonio]-1-propanesulfonate hydrate (CHAPS), 0.00813M, 5%; Heparin, 100 µg/mL; and ultrapure $H_2O$]. Afterwards, lungs were incubated for at least one hour with the hybridization solution at 70˚C. Finally, the lungs were incubated with DIG-RNA labeled probe mixed in the hybridization solution at a final concentration of 0.5%, at 70˚C overnight.

On the following day, the probe was retrieved, and tissues were washed twice with pre-heated hybridization solution at room temperature and once at 70˚C (30 minutes). Next, tissues were washed with hybridization solution plus MABT [MAB 5x (Maleic Acid, 0.5M; NaCl, 0.74M; NaOH, pH 7.5) diluted 5 times; Tween 20, 10%; ultrapure water]. Then, tissues were incubated with a blocking solution [blocking reagent (Roche Applied Sciences) 2% and goat serum (Invitrogen) 20% in MABT], to decrease the background. Finally, tissues were incubated overnight, at room temperature and with gentle agitation, with anti-digoxigenin antibody solution (1:2000 in blocking solution; Roche Applied Sciences).

On the third day, several washes with MABT were carried out and after tissues were washed twice with NTMT (NaCl, 0.1M; Tris-HCl, 0.1M; $MgCl_2$, 50mM; and Tween 20, 1%). Then, tissues were incubated with developing solution containing blue 4-nitro tetrazolium chloride (NBT) and 5-bromo-4-chloro-3-indoyl-phosphate (BCIP) in NTMT. In the presence of NBT, the alkaline phosphatase (bound to the anti-digoxigenin antibody) cleaves BCIP thus promoting the formation of a blue precipitated in the sites where the enzyme is present. The developing reaction was stopped, at the same time, for the same group of

tissues, by washing 3 times in PBT. Tissues were photographed with a camera Olympus U-LH100HG coupled to a stereomicroscope Olympus SZX16 and stored at 4°C.

## 3.8. Quantitative real-time polymerase chain reaction (qRT-PCR)

qRT-PCR is a highly sensitive and reproducible technique used to detect and quantify mRNA levels. The procedure is based on the fluorescence labeling of the amplified PCR product. During each cycle, the fluorescence is measured and the signal increases proportionally to the amount of PCR product amplified and, hence, it is quantified in "real-time". The fluorescent signal is generated by the presence of DNA-binding dyes that allow identifying the exponential phase of the reaction[124].

### 3.8.1. RNA extraction and quantification

Lung explant tissue was retrieved from -80˚C and placed on ice. Total RNA was extracted from D0 and D2 lung explants, from three culture conditions, using TripleXtractor direct RNA kit (GRiSP) according to the manufacturer's instructions. Next, total RNA was quantified using Nanodrop. Finally, RNA was analyzed through an Experion automated electrophoresis system (Bio-Rad) to assess RNA integrity and purity, using the Experion RNA StdSens kit (Bio-Rad).

### 3.8.2. DNase treatment

Total RNA was treated with DNase to remove genomic DNA from the sample. Total RNA was incubated with DNase-RNase free (Thermo Fisher Scientific) following the manufacturer's guidelines. Briefly, after 30 minutes, at 37˚C, the reaction was stopped with EDTA and the enzyme inactivated for 10 minutes, at 65˚C.

### 3.8.3. cDNA synthesis and quantification

cDNA was obtained from treated RNA (<5 µg) using GRS cDNA Synthesis kit (GRiSP) respecting manufacturer's protocol for oligo(dT)$_{20}$ primers. Samples were quantified using the Nanodrop and stored at -20˚C. To validate cDNA quality, GAPDH was amplified by conventional PCR using KAPA2G Fast ReadyMix PCR Kit (KAPA Biosystems, USA) and forward and reverse GAPDH primers (Forward: 5'-ATATGACAAGTCCCTGAAAATTGTCAG-3'; Reverse: 5'-GCATCAAAGGTGGAGGAATGG-3').

### 3.8.4. qRT-PCR

The primers used in this study (Table 1) had already been previously optimized for annealing temperature, cycles and cDNA dilution (to ensure similar efficiency range). qRT-PCR was performed using 1 µL of cDNA sample (70 ng/µL), and NZY qPCR Green Master Mix (2x) (NZYTech, Portugal), according

to manufacturer's instructions. mRNA expression levels were normalized for two housekeeping genes: *18S* and *β-actin*. Each sample was run in duplicate (n=8/condition). Relative gene expression was calculated following the mathematical model 2^(ΔCt), being $\Delta Ct=Ct_{reference}-Ct_{sample}$. Additionally, fold variation of gene expression levels was calculated following the mathematical model 2^(-ΔΔCt)[125], being $\Delta\Delta Ct=\Delta Ct_{sample}-\Delta Ct_{control}$. All quantitative data are presented as mean ± SEM with a statistically significant level of 5% ($p<0.05$). Statistical analysis was performed using GraphPad Prism 6 (USA). Normality of distribution and homogeneity of group variances were tested, and One-Way ANOVA was performed.

**Table1. List of primers and qRT-PCR conditions.** Forward and reverse primer sequences, number of qRT-PCR cycles and annealing temperature.

| Gene | Primers (5'-3') | Number of cycles | Annealing temperature |
|---|---|---|---|
| *18S* | TCTTTCTCGATTCCGTGGGT<br>AACGCCACTTGTCCCTCTAC | 35 | 58˚C |
| *β-actin* | CTTCTAAACCGGACTGTTACCA<br>AAACAAATAAAGCCATGCCAATCT | 35 | 58˚C |
| *ldha* | AAGACGCCGGCAGTACAC<br>GAGTGTGCAGTCACGCTGTA | 35 | 58˚C |
| *ldhb* | ACTTGGTATCCACCCAACCAG<br>CTCAGCAACGCTAAGACCAAT | 35 | 54˚C |
| *pdha* | TCACGGCTTTACCTATGCCC<br>ACCTGAGCACCGACAATACC | 35 | 58˚C |
| *pdhb* | GCTCAGAAGATGCTAAAGGGC<br>GCTTCTAAACAGTGCCCAACAG | 35 | 58˚C |
| *hk1* | CTGGCCTACTACTTCACCGAG<br>TCACTGTCGCTGTTGGGTTA | 40 | 58˚C |
| *hk2* | GCGCAGAAGGTGGACAAATAC<br>TGCCAAGAAGTCTCCGTCCT | 45 | 58˚C |
| *glut1* | GCAGTTCGGCTACAACACCG<br>ATCAGCATGGAGTTACGCCG | 40 | 58˚C |
| *glut3* | GTACCGTTCGGGTTCCGTTAG<br>AATGGCAGCAACAGAAACAGC | 40 | 62˚C |
| *glut8* | AGCTTTGGCTTCGTGCTAGG<br>GTAGCCTCCCAGTATTCCTCC | 40 | 58˚C |
| *mct1* | TCGGAGCCTTCATCTCCATTG<br>CAATCAAACCACACCCCGAG | 40 | 58˚C |
| *mct4* | GGATCTGCACTCAGGGAACC<br>GGAAAGGCGTAGGAGAACCC | 45 | 62˚C |
| *mct8* | TTCTTCTGCTCTCCCATCGT<br>CGACGCTTGAAGTAGTGACC | 40 | 58˚C |

## 3.9. Metabolite analysis

Metabolomics is defined as the analysis of small molecules involved in the metabolism of living organisms, the metabolites. Metabolites present a molecular weight below 1800-1500 Dalton and can act as substrates or products on different metabolic pathways. This class of compounds includes sugars, amino acids, and lipids amongst others and are related not only with the cellular energetic machinery but also with intercellular communication[126]. The metabolome provides insights about specific metabolic, biochemical and molecular alterations since it is the reflex of all the reactions occurring in cells and tissues.

Currently, the two major approaches used are targeted and untargeted metabolomics. The targeted method focuses on specific metabolites, metabolic pathways or compound classes based on the specific chemical properties of the targeted metabolites. On the other hand, the untargeted approach aims the coverage of all metabolites existing in the sample without previous biological knowledge[127]. Proton NMR ($^1$H-NMR) spectroscopy allows absolute quantification, metabolite identification, and reduced interference and it is widely used for these studies.

### 3.9.1. Extracellular medium analysis

Samples of culture medium (≈ 200 µL) from D0, D1, and D2 (section 3.3) were analyzed by $^1$H-NMR spectroscopy (n=6/condition/stage) and injected directly. In order to quantify the extracellular metabolites in the media, sodium fumarate (singlet, at 6.50 ppm, $\delta$ parts per million), was used as an internal reference. Spectral acquisition was performed at 14.1T and 25˚C using a Bruker Avance 600 MHz spectrometer equipped with a 5-mm QXI probe and a z-gradient, with solvent-suppression and a sweep width of 6 kHz, using a delay of 14 seconds, a water presaturation of 3 seconds, a pulse angle of 45˚, an acquisition time of 3.5 seconds and at least 128 scans[128] The following metabolites were quantified: histidine (doublet, 7.9 ppm), phenylalanine (double doublet, 7.4 ppm), tyrosine (multiplet, 6.9 ppm), glycine (singlet, 3.54 ppm), choline (singlet, 3.18 ppm), H1-$\alpha$ glucose (doublet, 5.22 ppm), glutamine (multiplet, 2.44 ppm), succinate (singlet, 2.39 ppm), acetate (singlet, 1.9 ppm), alanine (doublet, 1.46 ppm), lactate (doublet, 1.33 ppm) and valine (doublet, 1.02 ppm). The relative areas of $^1$H-NMR resonances were quantified using the curve-fitting routine supplied with the NUTSproTM NMR spectral analysis program (Acorn NMR, USA). The concentration of the different compounds was obtained according to the following formula ($A_{compound}$ corresponds to the peak(s) area in the $^1$H-NMR spectra).

$$[\text{Compound}] = \frac{[\text{Fumarate}] \times (A_{\text{Compound}} / \text{Number of Protons}_{\text{Compound}})}{(A_{\text{Fumarate}} / \text{Number of Protons}_{\text{Fumarate}})}$$

Absolute quantification (pmol) was normalized over lung growth ratio (epithelial perimeter) (section 3.8.1).

### 3.9.2. Tissue metabolite analysis

Three pools of 50 mg of whole lung tissue (roughly 70 stage b2 lungs/pool) were collected on ice and kept at -80°C. Next, tissues were lyophilized, weighted, and kept at -80°C for further metabolite extraction. Briefly, 1 mL of methanol:chloroform mixture (2:1) was added to the lyophilized samples and tissues sonicated at 4˚C for 15 minutes. Afterwards, 500 µL of chloroform and an equal volume of water were added and mixed thoroughly by vortexing. Finally, the samples were centrifuged, 10000g, for 20 minutes at 4˚C. The aqueous phase, containing the water-soluble metabolites was collected and stored at -80˚C. Lastly, samples were lyophilized and weighted. Before loading the sample in the equipment, sodium fumarate was added as an internal reference as described in the previous section (3.9.1).

With the standard parameters, a database was created, and the samples were loaded into the machine.

Spectral analysis was performed with the NUTS NMR Data Processing Software (Acorn NMR Inc.). The following metabolites were quantified: adenosine monophosphate (singlet, 8.57 ppm), inosine monophosphate (singlet, 8.54 ppm), formate (singlet, 8.44 ppm), adenosine (singlet, 8.33 ppm), adenosine triphosphate (singlet, 8.25 ppm), glutamate (double doublet, 3.74 ppm), glycine (singlet, 3.54 ppm), taurine (triplet, 3.40 ppm), O-phosphocholine (singlet, 3.2 ppm), creatine (singlet, 3.02 ppm), succinate (singlet, 2.39 ppm), pyruvate (singlet, 2.36 ppm), acetate (singlet, 1.9 ppm), alanine (doublet, 1.46 ppm) and lactate (doublet, 1.33 ppm). The concentration of the different compounds was obtained according to the previously described formula (section 3.9.1), and the absolute quantification (pmol) was normalized by the weight of lyophilized tissue.

# 4. Results

Lung development is a highly complex process that depends on the crosstalk between several signaling pathways that ultimately contribute to proper branching morphogenesis. Hippo signaling has recently emerged as a key player in lung organogenesis and it is known to be involved in organ size control, tissue regeneration, and homeostasis. Contrasting with the extensive knowledge about the molecular mechanisms underlying lung branching is the almost absence of data regarding the interaction between signaling and metabolism in the early stages of lung development.

In this work, we aimed to clarify the role of Hippo signaling in regulating lung growth and metabolism, specifically through its effector TAZ (a transcriptional co-activator with PDZ-binding domain). For this purpose, *in vitro* lung explants were cultured with a TAZ nuclear translocational enhancer (TM-25659) that promotes TAZ nuclear localization and, consequently, its association with transcription factors like the TEAD or RUNX2. Explants were morphometrically analyzed to determine the impact on lung growth. Lung tissue was collected for determining the expression levels of selected glucose catabolism genes, by qRT-PCR. Culture medium was collected and extracellular metabolites analyzed and quantified, by $^{1}$H-NMR spectroscopy.

## 4.1. *In vitro* TAZ modulation in the embryonic chick lung

To clarify the role of TAZ during early stages of chick lung branching morphogenesis, *in vitro* lung explants were treated with TM-25659, and doses selected according to the literature (5 μM, 10 μM, 15 μM, 20 μM). DMSO served as a control since the drug was dissolved in this solvent. TAZ impact on pulmonary growth was assessed by morphological analysis, and TAZ modulation confirmed by *in situ* hybridization, for *runx2*.

### 4.1.1. Impact of TAZ modulation in lung branching and growth

Stage b2 lungs were cultured for 48 hours with increasing doses of TAZ and with DMSO (Fig 3). In figure 3 it is possible to observe that treated lung explants (Fig 3D, 3F, 3H and 3J) display normal growth when compared to control explants (Fig 3B).

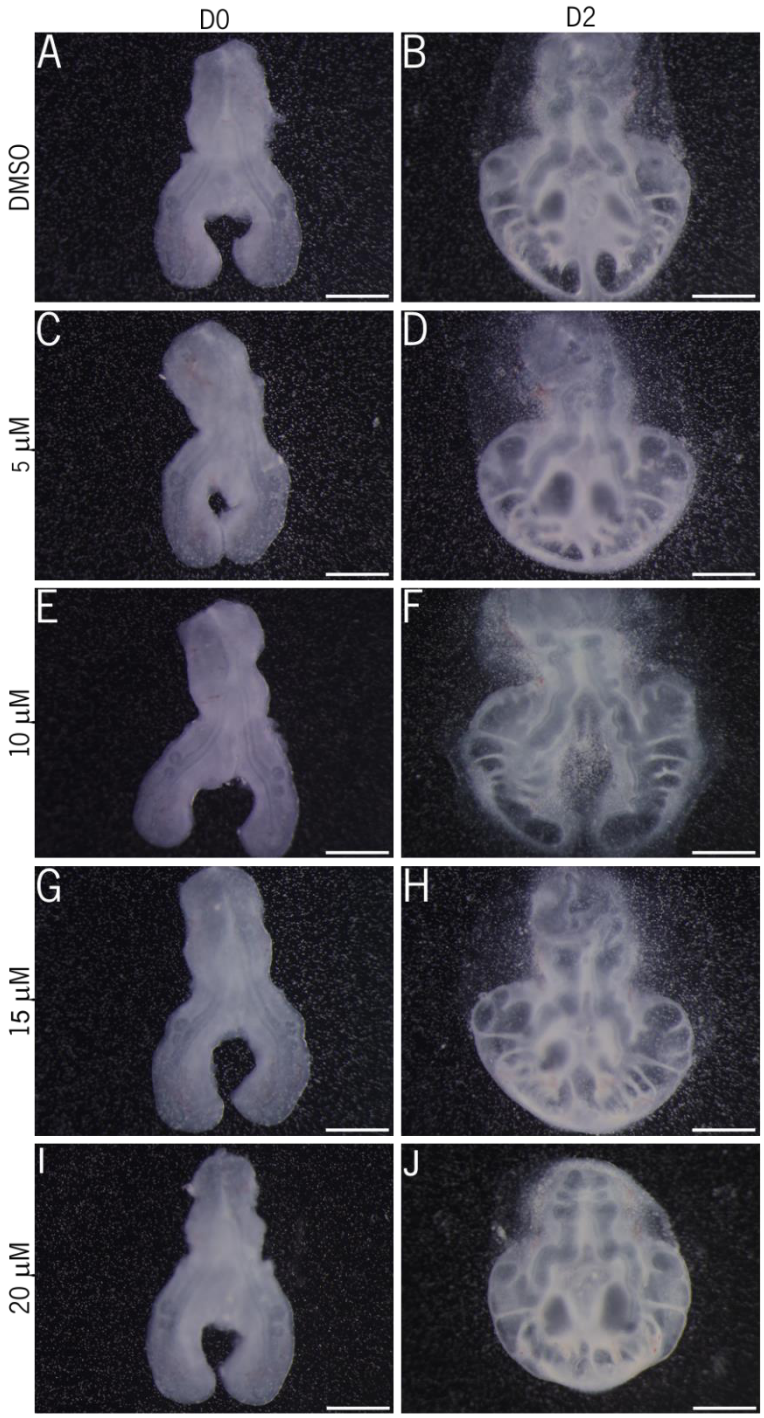


**Figure 3. *In vitro* chick lung explant culture.** Representative examples of stage b2 lung explants at 0h, D0 (A, C, E, G and I) and after 48h of culture, D2 (B, D, F, H and J) in control (DMSO) or TM-supplemented (5, 10, 15 or 20 µM) media. Scale bar: 500 µm.

In order to study the impact of TAZ manipulation in lung growth, cultured lung explants were assessed morphometrically at 0h and 48h. A specific set of parameters was measured allowing to determine the effect in both mesenchymal and epithelial compartments, namely, epithelial and mesenchymal areas and perimeters. Moreover, the number of secondary airway buds was determined in order to evaluate lung branching. Results are presented as D2/D0 ratio.

The branching analysis (Fig 4A) revealed that there were no differences between DMSO and the lowest (5 μM) and the highest (20 μM) dose. Conversely, a significant increase in branching was detected in the 10 μM and 15 μM-treated explants, when compared with the control (10.5% and 12.1%, respectively). Moreover, 10 and 15 μM-treated explants displayed a significant increase when compared with the lowest dose (15.1% and 16.7%, respectively). Regarding total area (Fig 4B), the morphometric evaluation revealed that there were no differences between groups, which implies that treatment did not affect the overall size of the lung.

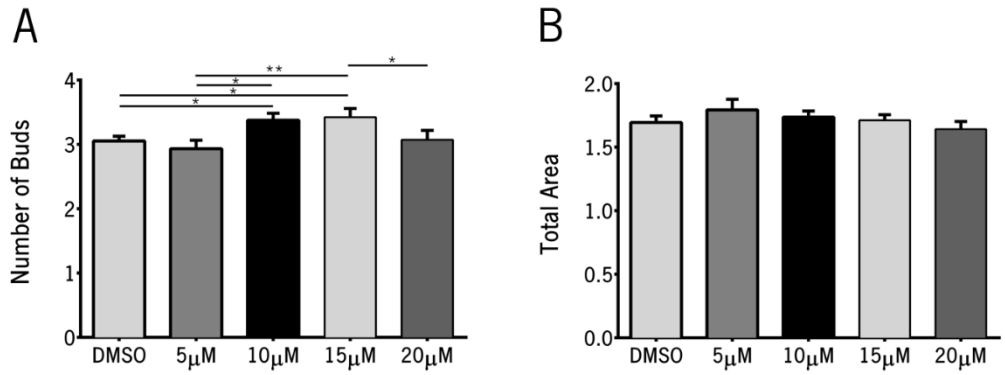


**Figure 4. Morphometric and branching analysis of stage b2 lung explants.** Control and TM-treated (5, 10, 15, 20 μM) lung explants were evaluated at D0 and D2 for: number of secondary buds (branching) (A) and total area (B); n≥15/condition. Results are expressed as D2/D0 ratio. The data is shown as mean ± SEM. p≤0.05: *; p≤ 0.01: **.

Concerning epithelial perimeter and epithelial area, no major differences were observed between control and TM-treated lungs (Fig 5). There are some differences in the epithelial area, namely between the 20 μM-treated explants *vs* 5 μM and *vs* 15 μM-treated explants (Fig 5A). Regarding the epithelial perimeter, only a 6% decrease was detected between 15 μM and 20 μM-treated explants (Fig 5B).

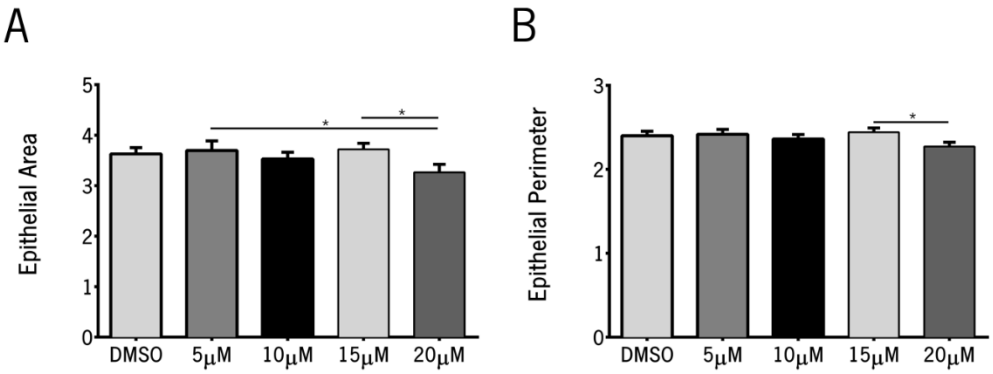


**Figure 5. Morphometric/Epithelial analysis of stage b2 lung explants.** Control and TM-treated (5, 10, 15, 20 μM) lung explants were evaluated at D0 and D2 for: epithelial area (Fig 5A) and epithelial perimeter (Fig 5B); n≥15/condition. Results are expressed as D2/D0 ratio. The data is shown as mean ± SEM. p≤0.05: *.

Considering the mesenchymal morphometric measurements, for the mesenchymal area, no differences were observed between DMSO and 5, 15 and 20 μM-treated explants, or among these doses (Fig 6A). In contrast, 10 μM-treated explants display a significant increase of 17.6% when compared with the control. Finally, a significant reduction of 14% was noticed in the 15 μM dose comparing to the 10 μM treatment. Regarding the mesenchymal perimeter no differences between control and treatment conditions were detected (Fig 6B). However, a significant decrease was noted between 20 μM *vs* 5 μM and *vs* 10 μM-treated explants.

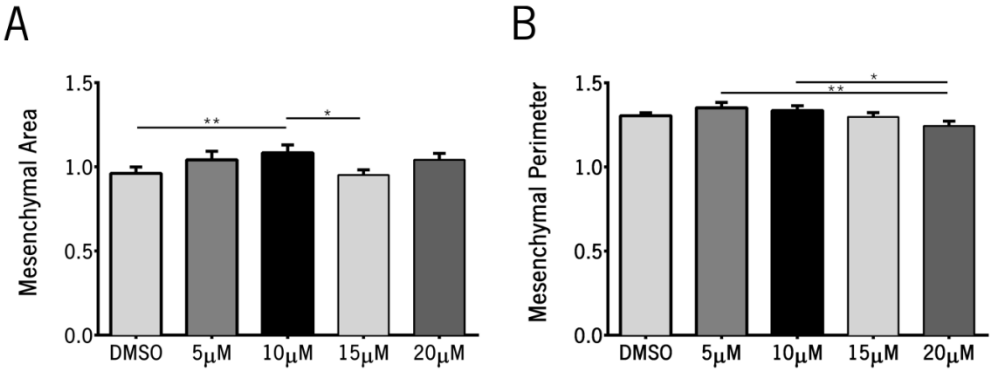


**Figure 6. Morphometric/Mesenchymal analysis of stage b2 lung explants**. Control and TM-treated (5, 10, 15, 20 μM) lung explants were evaluated at D0 and D2 for: mesenchymal area (Fig 6A) and mesenchymal perimeter (Fig 6B); n≥15/condition. Results are expressed as D2/D0 ratio. The data is shown as mean ± SEM. p≤0.05: *; p≤ 0.01: **.

### 4.1.2. Impact of TAZ modulation in total YAP and TAZ protein levels

TM-25659 enhances TAZ nuclear localization, in a dose-dependent, manner without affecting the total amount of TAZ in pluripotent C3H10T1/2 cells[129]. In this sense, to confirm if the total amount of TAZ protein remained unchanged after treatment, the expression levels of TAZ were evaluated by Western blot (Fig 7). Additionally, the expression levels of total YAP were also assessed to certify the specificity of this treatment. In figure 7A, a representative example of a western blot for both proteins, after 48 hours in culture, is displayed. β-tubulin served as a loading control. The expression levels of both YAP and TAZ seem very similar.

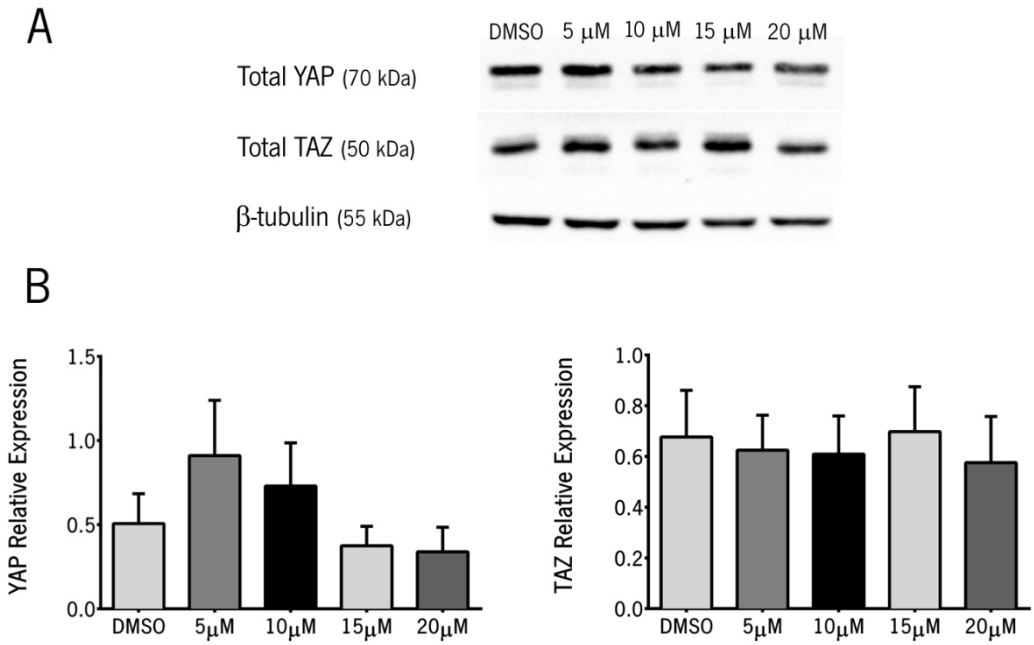


**Figure 7. Total YAP and total TAZ protein expression levels.** (A) Western blot analysis of total YAP and total TAZ in control (DMSO) or TM-supplemented (5, 10, 15 or 20 μM) chick lung explants. Control loading was performed using β-tubulin. (B) Semi-quantitative analysis for total YAP and total TAZ, after 48 hours in culture (D2). The results are presented in arbitrary units normalized for β-tubulin, mean ± SEM (n=3/condition).

The semi-quantitative analysis revealed that YAP and TAZ protein levels remain stable, regardless of the treatment, and there are no statistically significant differences between control and treated-lungs (Fig 7B). These results demonstrate that TM-25659 does not affect total protein levels.

### 4.1.3. Validation of TAZ translocation by *in situ* hybridization for *runx2*

RUNX2 is a transcription factor that is a known target of YAP and TAZ [130]. TAZ is required for mesenchymal lineage commitment by interacting with RUNX2[131]. Additionally, YAP nuclear translocation

into the nucleus promotes Runx2 suppression whereas TAZ translocation promotes its activation[132]. Therefore, *runx2* is considered a specific target of TAZ.

To verify if *runx2* expression is altered, thus confirming TAZ nuclear translocation, we first ought to characterize its expression pattern in early branching stages namely, b1, b2, and b3 (Fig 8A-C). This was the first time that *runx2* expression was described in this tissue.


**Figure 8. Characterization of *runx2* expression by *in situ* hybridization.** Representative examples of *in situ hybridization* for *runx2* in embryonic chicken lungs stage b1 (A), b2 (B) and b3 (C) (n=5/stage). Scale bar: 500 μm.

*runx2* mRNA was detected in all stages analyzed; nonetheless, its expression levels were relatively low in all stages (Fig 8A-C). *runx2* is expressed in the epithelial compartment, particularly in the proximal epithelium of the trachea region. Moreover, it is also present adjacent to the sites where the secondary buds start to sprout. The expression is absent from the distal epithelium and mesenchyme. Whole embryos displayed a strong expression in the limbs as expected (Fig 18-Appendix 1) thus validating the results for the lung.

After characterization, *runx2* expression where assessed in TM-treated explants, by *in situ* hybridization (Fig 9). From this point onwards, only 10 μM and 15 μM doses of TM-25659 were used taking into consideration that these doses display statistical differences in branching when compared to control (Fig 4A).

*In situ* hybridization revealed that there is a slight increase in the expression of *runx2* transcript 10 and 15 μM-treated explants (fig 9F and 9I, respectively) when compared to control explants (Fig 9C). Furthermore, no major differences were observed between different the two selected doses (Fig 9F and 9I). *In situ* hybridization confirmed that TAZ is fact being translocated into the nucleus and it is activating its specific-gene expression program.

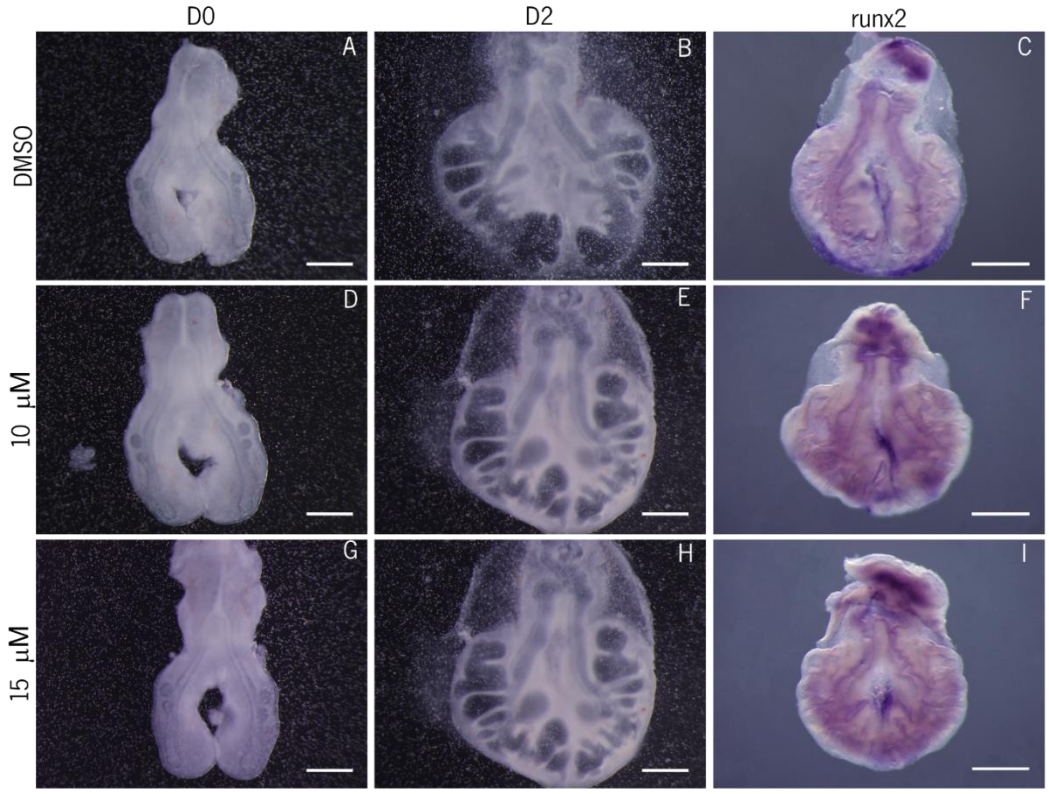


**Figure 9.** ***In situ*** **hybridization for** ***runx2*****.** Embryonic chicken stage lungs b2 at 0 hours (D0) (A, D and G); after 48 hours (D2) of culture with DMSO (B), 10 µM (E) and 15 µM (H). Same lung explants after the *in situ* hybridization protocol (C, F and I) (n=5/condition). Scale bar: 500 µm.

## 4.2. Impact of TAZ manipulation on the expression levels of key metabolic enzymes and transporters

Glucose catabolism is thought to be the main energy source for the developing embryo and, therefore, for the developing lung. To determine the effect of TAZ nuclear translocation in the expression levels of metabolism-related genes, qRT-PCR was performed for: transporters, *glut1*, *glut3* and *glut8* (Fig 10) and *mct1*, *mct4* and *mct8* (Fig 11); and enzymes, *hk1* and *hk2* (Fig 12); *pdha* and *pdhb* (Fig 12); and *ldha* and *ldhb* (Fig 13). Specific primers were already available and optimized for annealing temperature and PCR cycles. mRNA expression levels were normalized for *18s* and *β-actin* housekeeping genes.

In figures 10 and 11, the relative expression values of glucose transporters (GLUT's) and monocarboxylate transporters (MCT's) are displayed. *glut1* and *glut8* expression levels exhibit the same increasing tendency, in a dose-dependent manner (Fig 10A and 10C). However, only *glut8* expression levels (Fig 10C) display a statistically significant difference between 15 µM dose when compared to both control and 10 µM-treated lungs, with a fold variation of 4.9 and 3.2, respectively. On the other hand,

*glut3* (Fig 10B) expression levels remained virtually unaffected by TM-25659 treatment, with no statistical differences between the three groups.

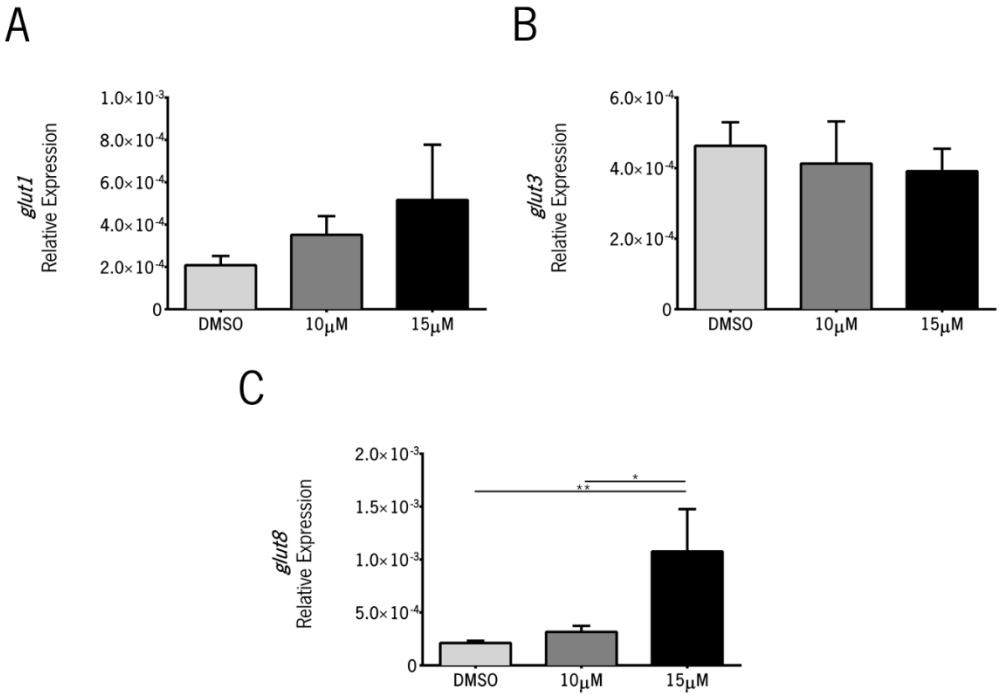


**Figure 10. mRNA expression levels of key glucose catabolism transporter genes after TAZ stimulation with TM-25659 for 48 hours.** Relative expression levels of *glut1* (A), *glut3* (B) and *glut8* (C). Results are expressed in arbitrary units, as mean ± SEM (n≥5/condition). p≤0.05: *; p≤ 0.01: **.

Regarding MCT's, *mct1* and *mct4* (Fig 11A and 11B) expression levels did not vary between conditions. Nevertheless, *mct8* expression levels (Fig 11C) presented a noteworthy, statistically significant and dose-dependent increase in the higher dose when compared to the control with a fold variation of 12.6.

*hk1* and *hk2* expression levels (Fig 12A and B) were moderately maintained in the three conditions, without statistical differences. Nonetheless, *hk2* (Fig 12B) expression levels displayed a clear increasing tendency in a dose-dependent manner.

*pdha* and *pdhb* transcripts (Fig 13A and B) presented a similar tendency with a substantial increase in the highest dose when compared to the control with a fold variation of 2 in both cases.

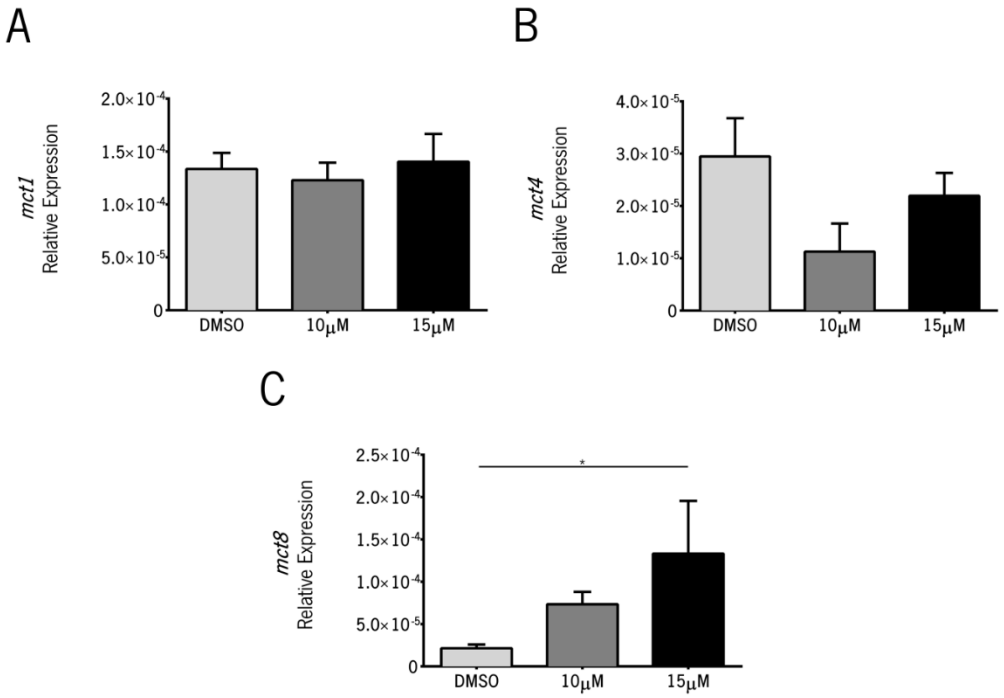


**Figure 11. mRNA expression levels of key glucose catabolism transporter genes after TAZ stimulation with TM-25659 for 48 hours.** Relative expression levels of *mct1* (A), *mct3* (B), and *mct8* (C). Results are expressed in arbitrary units, as mean ± SEM (n≥5/condition). p≤0.05: *.

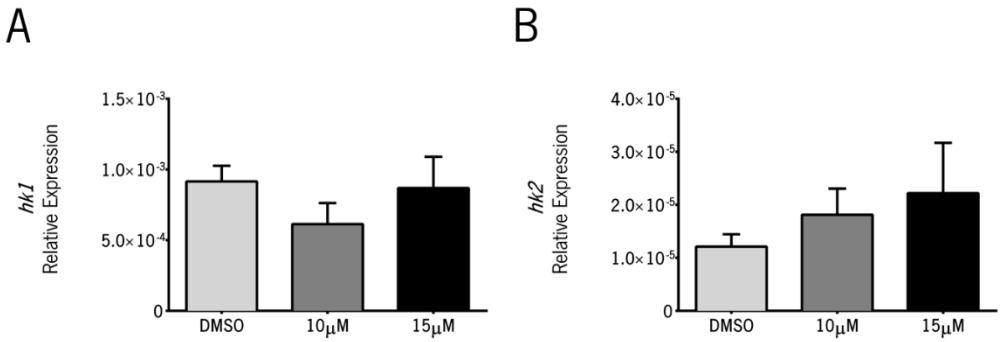


**Figure 12. mRNA expression levels of key glucose catabolism enzyme genes after TAZ stimulation with TM-25659 for 48 hours.** Relative expression levels of *hk1* (A) and *hk2* (B). Results are expressed in arbitrary units, as mean ± SEM (n≥5/condition).

Regarding *ldha* (Fig 14A) and *ldhb* (Fig 14B), an increase in the expression levels was detected for the highest dose when compared to the control. In terms of fold variation, a 6.2 and 2.6 increase were detected for ldha and ldhb respectively. Additionally, for *ldha*, there was also an evident increase between 10 μM and 15 μM dose of about 2.93 in fold variation.

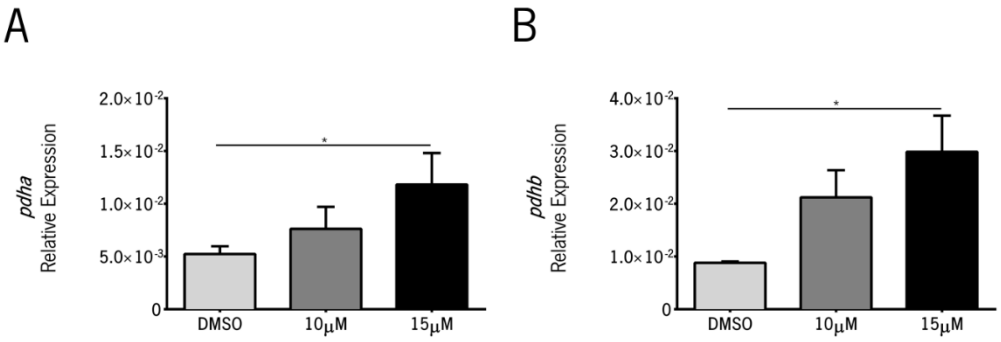


**Figure 13. mRNA expression levels of key glucose catabolism enzyme genes after TAZ stimulation with TM-25659 for 48 hours.** Relative expression levels of *pdha* (A) and *pdhb* (B). Results are expressed in arbitrary units, as mean ± SEM (n≥7/condition). p≤0.05: *.

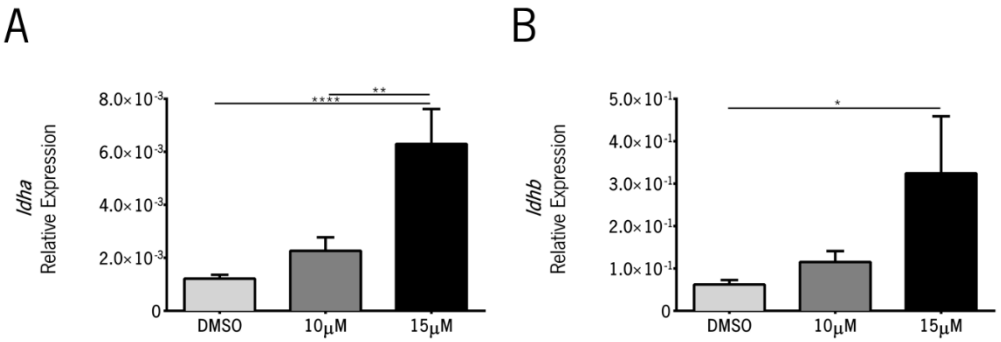


**Figure 14. mRNA expression levels of key glucose catabolism enzyme genes after TAZ stimulation with TM-25659 for 48 hours.** Relative expression levels (A and B) of *ldha* and *ldhb*. Results are expressed in arbitrary units, as mean ± SEM (n≥7/condition). p≤0.05: *; p≤ 0.01: **; p≤ 0.0001: ****.

## 4.3. Impact of TAZ manipulation in the extracellular metabolite profile of the developing lung

To characterize the metabolic alterations associated with TAZ manipulation, the medium from *in vitro* lung explant cultures treated with DMSO, 10 and 15 μM TM-25659 was collected, and extracellular metabolite fluctuations assessed by $^{1}$H-NMR spectroscopy. With this approach, we were able to detect, in the extracellular medium: acetate, alanine, choline, glucose, glycine, histidine, lactate, phenylalanine, succinate, tyrosine and valine. Metabolite production/consumption was expressed in pmol per growth ratio (Fig 15 and 19-Appendix 1). As a reference, normal supplemented medium (without DMSO or TM-25659) was used.

The $^{1}$H-NMR results revealed that glucose consumption (Fig 15A) and lactate production (Fig 15B) remained unaltered, regardless of the treatment. Alanine (Fig 15C) was produced although there are no statistically significant differences between treatments. Glutamine consumption (Fig 15D) increases

mildly, in a dose-dependent manner but without statically significance. Conversely, a progressive and dose-dependent increase in acetate (Fig 15E) and succinate (Fig 15F) production is observed, that reaches its maximum in the 15 µM condition when compared to the control. Regarding other metabolites including, histidine, phenylalanine, tyrosine, glycine, choline and valine, no differences were observed between treatments (please see Fig 19-Appendix 1).

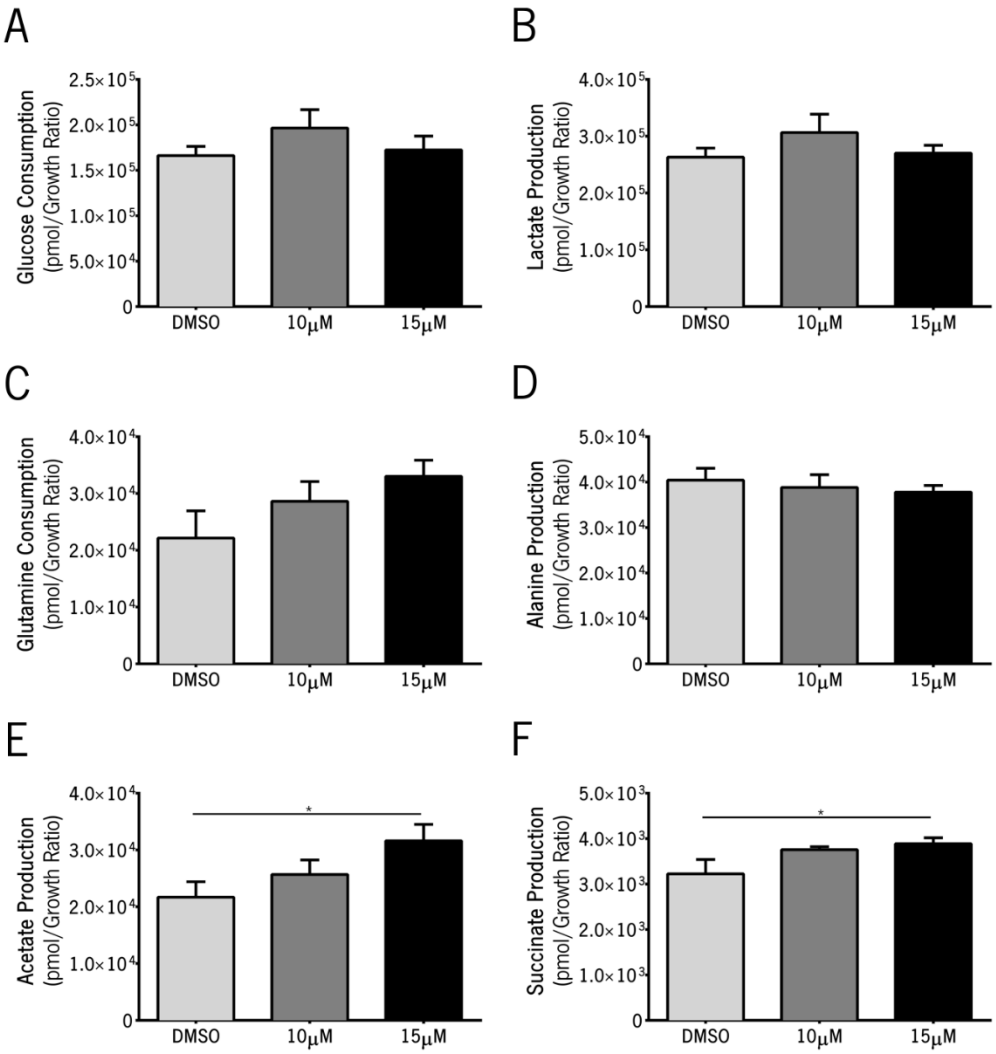


**Figure 15. Metabolite concentration after TAZ stimulation with TM-25659 for 48 hours.** Representation of glucose consumption (A), lactate production (B), glutamine consumption (C), alanine production (D), acetate production (E) and succinate production (F). Results are expressed as mean ± SEM (n≥6/condition). p≤0.05: *

## 4.4. Embryonic lung tissue metabolomic profile

Lung embryonic metabolic signature has not been described in the literature before. In this sense, we characterized the normal metabolomic profile of stage b2 lungs by $^{1}$H-NMR spectroscopy. From the $^{1}$H-NMR spectra, we were able to detect metabolites that belong to different families of biomolecules,

namely, amino acids, nucleotides, and intermediaries of glycolysis and Krebs cycle. However, glucose was not detected. Results are presented in figure 16.

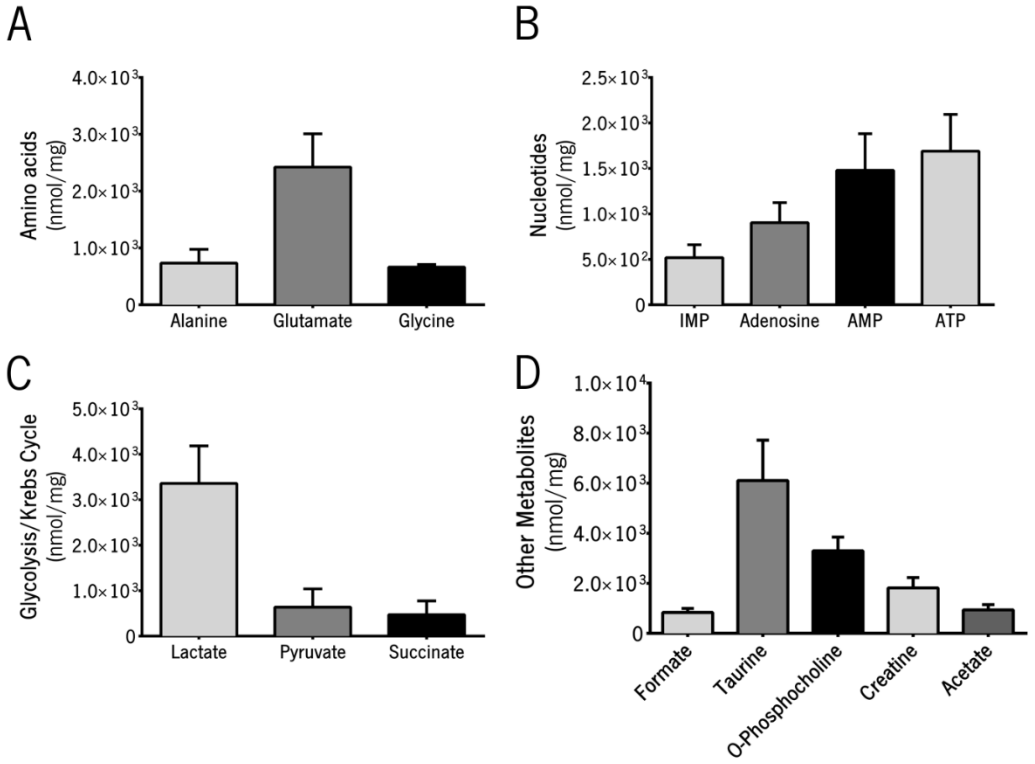


**Figure 16. Metabolomic analysis of the embryonic chicken lung.** Metabolite quantification of embryonic chicken lung stage b2. Metabolites were grouped in families: amino acids (A), nucleotides (B), glycolysis/Krebs cycle intermediaries (C) and other metabolites present in high amounts (D) Results are expressed as mean ± SEM (n=3/condition).

Considering amino acids (Fig 16A), we were able to identify and quantify alanine, glutamate, and glycine. Among them, glutamate is present in a considerably higher amount than its counterparts. Regarding nucleotides (Fig 16B), we detected the presence of inosine monophosphate (IMP), adenosine, adenosine monophosphate (AMP) and adenosine triphosphate (ATP). From glycolysis and Krebs cycle (Fig 16C) we detected lactate, pyruvate, and succinate. The amount of lactate present in the tissue was significantly higher than pyruvate and succinate levels. Furthermore, other metabolites (Fig 16D) like acetate, formate, taurine, O-phosphocholine, and creatine were also identified and quantified.

# 5. Discussion

Hippo signaling is a highly conserved signaling pathway that influences many important biological processes during the development of tissues and organs, among them the lung. This pathway is responsible for controlling several cellular events like the regulation of cell growth, proliferation, survival, and organ-size control; more recently, it has been also implicated in metabolic regulation. The molecular mechanisms underlying lung branching morphogenesis have been well described during lung development, however, the interplay between Hippo effectors and metabolism in early lung development has not been addressed so far. The work presented in this Master thesis aimed to dissect the role of Hippo effector TAZ in the regulation of the metabolic program of the embryonic lung.

## 5.1. TAZ nuclear localization and influence in lung branching and growth

*Ex vivo* explant culture is one of the best techniques to study organogenesis-related events since it maintains native interactions between cells within tissues. In this study, we selected TM-25659 that enhances TAZ nuclear translocation in a dose-dependent manner, without changing the total TAZ protein level in the cells[129].

Stimulation of TAZ nuclear translocation in lung explants did not promote morphological alterations when compared to control explants (Fig 3). Considering lung branching, a mild increase in the number of secondary buds formed, after 48 hours, for the 10 μM and 15 μM doses was detected. No significant differences were observed for the 5 μM and 20 μM treatments when compared with the control. Despite this mild increase in branching, the overall size of the lung is maintained (Fig 4B). Moreover, no major differences were observed in the perimeter and area of lung compartments (epithelium/mesenchyme) individually. Altogether, these results suggest that secondary buds formed are smaller when TAZ is translocated to the nucleus. Branching morphogenesis relies on the crosstalk between epithelial and mesenchymal compartments mediated by signaling pathways. Among them, FGF plays a crucial role in this event. In fact, perturbations in this signaling pathway causes abrogation of branching[3]. Additionally it has been demonstrated that during processes of homeostasis or injury, basal stem cells have the ability to downregulate their Hippo signaling, (increasing YAP/TAZ nuclear localization) to generate their own localized Fgf10-expressing niche[69,133,134]. In our experimental setting, an interaction between Hippo and FGF signaling may account for the observed increase in branching.

## 5.2. Molecular validation of TAZ manipulation

It has been described that TM-25659 enhances TAZ nuclear translocation without altering the total TAZ protein levels in the cells[129]. To confirm TAZ manipulation, the expression levels of total TAZ protein were assessed, by Western blot, in lung explants treated with TM-25659 (Fig 7). Moreover, total YAP expression levels were also evaluated to discard a possible interference of the treatment with this effector. The Western blot analysis revealed that, regardless of the dose, total TAZ protein levels remain unchanged. This result is in accordance with the existing literature that claims similar results for the pluripotent embryonic C3H10T1/2 cell line. The authors found that TM-25659 significantly increased the nuclear localization of TAZ without changing its total amount probably due to reduced tyrosine phosphorylation; moreover, a direct interaction between the drug and TAZ protein has been suggested to induce conformational changes on TAZ however, the underlying mechanism is not clear. Moreover, TM-25659 treatment aided the DNA-binding activity of RUNX2 in the presence of TAZ[129]. Our results showed that total YAP protein levels remained unaltered, independently of TAZ stimulation, implying that there were no compensation events due to YAP and TAZ homology and shared transcription factors. This led us to conclude that the observed morphological effect is not related to an increase of protein expression levels but with the TAZ translocation into the nucleus and, consequently, activation of its gene expression program. Taking into consideration branching and protein expression data, from this point onwards, only two doses of TM-25659 were used: 10 and 15 μM.

TAZ nuclear localization was confirmed by *in situ* hybridization for *runx2,* one of the many transcription factors that interact with YAP and TAZ. However, nuclear localization of either YAP or TAZ differently impacts on *runx2* expression. YAP nuclear translocation promotes *runx2* suppression whereas TAZ nuclear localization promotes its activation[132]. RUNX2 belongs to the RUNX family of transcription factors, characterized by its DNA-binding domain runt and consists of three members, RUNX1, RUNX2, and RUNX3. RUNX2 is mainly expressed in osteoblasts[134] and chondrocytes[135], but also in uncommitted mesenchymal cells[136]. In humans, *runx2* encodes two isoforms RUNX2-type I and RUNX2-type II[137]. These two isoforms are differentially distributed in both space and time but also amongst different tissues and species. Both isoforms have already been described in adult bone and lung, whereas type I isoform is broadly expressed in heart, brain, skeletal muscles and spleen[138,139].

We characterized for the first time *runx2* expression pattern on embryonic chicken lung, by *in situ* hybridization (Fig 8). Our results showed that *runx2* mRNA is present in early stages of lung development namely, in b1, b2, and b3 stages; moreover, the expression levels were relatively low and there were no

major differences between stages. *runx2* is expressed more evidently in the proximal epithelium, similarly to *taz* expression pattern, and close to bud sprouting sites. Regarding *in vitro* explants, 10 and 15 μM of TM-25659 treated lungs display a mild increase in *runx2* expression when compared with the control. Altogether these results highlight that TAZ is being translocated into the nucleus, interacting with transcription factors and, consequently, promoting the expression of its target genes.

## 5.3. TAZ-induced alterations in glucose catabolism-related gene expression

Glucose catabolism is thought to be the main energy source for the developing embryo and therefore for the developing lung. To verify if TAZ nuclear translocation promoted alterations in the metabolism-related gene expression, qRT-PCR was performed for certain key transporters and enzymes involved in glucose catabolism.

The facilitated diffusion of sugars into cells is mediated by membrane proteins of the GLUT family (GLUT1–12 and GLUT14)[140]. We evaluated the expression levels of *glut1*, *glut3* and *glut8*. *glut1*; and *glut3* expression levels did not change with TM-treatment. Conversely, *glut8* expression increased in a dose-dependent manner, when compared to the control, and displayed a statistically significant difference for the 15 μM dose. GLUT8 is mainly an intracellular hexose transporter, however, there is conflicting evidence regarding GLUT8 localization in lysosomes (more plausible)[141], endoplasmic reticulum and microsomal membranes[142]. Notwithstanding, a study performed in blastocysts shown its localization in the plasma membrane after insulin stimulation[143]. Moreover, it can move between intracellular vesicles and the plasma membrane. Altogether, data presented on the literature points to the fact that GLUT8 is a constitutively intracellular hexose transporter that may be responsible for promoting transport of sugars or sugar derivatives into or out of intracellular organelles[144]. GLUT8 has a ubiquitous distribution and can partially substitute GLUT4 whose expression is less widely distributed[145]. It is conserved in chicken and its expression is ubiquitous as well. Although *glut8* expression is higher in kidneys and adipose tissue it has also been detected in the brain, adrenal, spleen, lung, testis, and pancreas. This transporter was shown to be insulin-responsive in the mammalian blastocyst, however, in rat adipose cells GLUT8 does not primarily function as an insulin-responsive transporter. In chicken, it is known to be an insulin-responsive glucose transporter[146–148]. 15 μM-treated explants display an increase in the expression levels of this transporter suggesting an increase in the intracellular glucose transport (since insulin is not present in the explant culture). Taking into consideration GLUT8 possible localizations, we may hypothesize that hexoses are being redistributed inside the cell to be used for biosynthetic purposes. Furthermore, developmental tissues require an intense synthesis of proteins; in this sense, intracellular glucose can be

used for protein glycosylation in the rough endoplasmic reticulum (RER). Concluding, intracellular hexose exchange may be supporting cellular biosynthesis, however, further studies focusing on this hypothesis are necessary.

MCTs are encoded by the family of genes SLC16A, with 14 members. MCT1-4 can perform proton-linked monocarboxylate transport whereas MCT8 is known to transport thyroid hormones[149]. We analyzed the expression levels of *mct1*, *mct4* and *mct8* (Fig 11). *mct1* and *mct4* expression levels remained constant in the lungs exposed to TAZ stimulation, without statistically significant differences compared to controls. On the other hand, *mct8* expression levels are significantly higher in 15 μM-treated explants when compared to control explants. MCT8 is a specific thyroid hormone cell-membrane transporter highly expressed in adult human tissues namely, in the liver, heart, brain, placenta, kidney and lung. The widespread distribution of this transporter is crucial since thyroid hormone is essential for the regulation of developmental and metabolic processes in many tissues. MCT8 is capable of transporting both 3,3',5-triiodothyronine (T3 or triiodothyronine) and 3',5',3,5 tetraiodo-L-thyronine (T4 or thyroxine)[150–153]. T4 is the main product of thyroid gland secretion and has low affinity for nuclear thyroid hormone receptors (TRs); contrarily, T3 has a high affinity for nuclear TRs and can be produced by the thyroid gland or in the neighboring area from T4 by target tissues and cells[153]. Thyroid hormones are known to stimulate the energetic metabolism especially on the muscle and liver promoting the expression of key catabolic enzymes[107]. MCT8 and MCT10 present a high degree of homology between them and have far less homology with the other members of the MCT family. This is mainly because MCT8 and MCT10 can transport amino acid derivatives whereas the other MCTs transport monocarboxylates. However, it has been proposed that other MCTs can also transport amino acids, and MCT8 and MCT10 can transport monocarboxylates as well[151]. Taking into consideration that thyroid hormones were absent from the culture medium, *mct8* increase may be due to the tissue necessity of transporting other monocarboxylates and/or amino acid derivatives (since it does not transport lactate) from and to the extracellular medium. This hypothesis corroborates the high biosynthetic and energetic activities which are characteristics of growing tissues such as the developing lung.

Besides glucose catabolism-related transporters, the expression levels of important enzymes were also assessed. We analyzed the expression levels of *hk1* and *hk2*; *pdha* and *pdhb*; and *ldha* and *ldhb*. The hexokinase family is composed of enzymes that irreversibly phosphorylate glucose into glucose-6-phosphate, at the expenses of one molecule of ATP. The phosphorylated form of glucose is trapped within the cells and enters its glycolytic fate[107]. *hk1* and *hk2* expression levels were not affected by the TM-25659

treatment and, so, it is likely that the total amount of glucose for catabolic metabolism entering the cells remains constant.

Pyruvate Dehydrogenase (PDH) is part of the mitochondrial pyruvate dehydrogenase complex (PDC) and uses pyruvate as its main substrate. PDC is a complex of three enzymes, pyruvate dehydrogenase (E1), dihydrolipoyl transacetylase (E2) and dihydrolipoyl dehydrogenase (E3). Pyruvate serves many destinations including the citric acid cycle after glycolysis but can be also converted into other molecules like glucose, glycerol, fatty acids, and non-essential amino acids[154]. PDH catalyzes the rate-limiting conversion of pyruvate into acetyl-CoA which can fuel different metabolic pathways[155]. Our results have shown an increase in both *pdha* and *pdhb* expression levels in a dose-dependent manner, statistically significant for the 15 µM treatment when compared with the control (Fig 13). The increase in gene expression of both *pdh* isoforms suggests a potential increase in the conversion of pyruvate into acetyl-CoA. Moreover, due to the irreversibility of the reaction, acetyl-CoA levels should increase and fuel other metabolic paths such as the Krebs cycle.

Lactate dehydrogenase (LDH) is a tetrameric glycolytic enzyme that catalyzes the reversible conversion of pyruvate to lactate, coupled with the oxidation of NADH to $NAD^+$. It comprises two major subunits, LDHA and LDHB which can form five different isoenzymes (LDH1, LDH2, LDH3, LDH4, and LDH5) by the different tetrameric associations between the two subunits. LDHA is the major form in skeletal muscle and presents higher affinity for pyruvate, thus converting pyruvate into lactate and producing $NAD^+$. LDHB is found mostly in heart muscle and converts lactate into pyruvate which then can be used for mitochondria oxidation. In the adult lung, LDH3 seems to be the most abundant isoenzyme[156]; this isoform is composed by two LDHA subunits and two LDHB subunits and presents intermediary enzymatic affinity meaning that it converts pyruvate into lactate or lactate into pyruvate[157–159]. *ldha* and *ldhb* expression levels exhibit a dose-dependent statistically significant increase when compared to control; this upsurge is more evident in the 15 µM dose (Fig 14). Furthermore, *ldh* expression results show that *ldhb* expression levels are 2 orders of magnitude higher than *ldha* ($10^{-1}$ *vs* $10^{-3}$), which points to LDHB as the main contributor in the embryonic lung. Taken together, these results point towards a potential metabolic shift from a glycolytic-lactate metabolic axis to the production of high amounts of pyruvate that can enter the Krebs cycle and, consequently, oxidative phosphorylation. This hypothesis is supported by the increased expression of both PDH isoforms and the fact that LDH catalyzes the interconversion between pyruvate and lactate, implying a potential pyruvate accumulation.

## 5.4. Characterization of the TAZ-induced metabolic profile

To determine whether TM-25659 treatment induced alterations in the embryonic lung metabolite profile, the extracellular medium from explant culture was analyzed by $^{1}$H-NMR spectroscopy. We were able to quantify glucose, lactate, glutamine, alanine, histidine, phenylalanine, tyrosine, glycine, choline, succinate, acetate, and valine (Fig 15 and Fig 19-Appendix 1). Glucose consumption and lactate production remained mostly unchanged and metabolite levels were quite similar to the control. We can conclude that TAZ manipulation did not affect glucose uptake from the medium neither the lactate export to the extracellular medium. Regarding the amino acids glutamine and alanine, their quantities in the medium remained constant; considering the amino acids histidine, phenylalanine, tyrosine, glycine, and valine no significant differences were detected. Choline production was not significantly altered by the treatment. Choline is an important water-soluble and vitamin-like nutrient that is a precursor of many of the main membrane phospholipids.

Regarding acetate, a significant increase in the 15 μM dose was detected, when compared to control. Acetyl-CoA is the precursor of acetate and can be produced by three main pathways, from pyruvate, fatty acids' β-oxidation and from ketogenic amino acids. Pyruvate is the final product of glycolysis and its oxidative decarboxylation by PDH generates acetyl-CoA[160] that can then originate acetate. The increase in the extracellular acetate levels seems to indirectly point to the intracellular formation of acetyl-CoA from pyruvate, followed by a transmembrane/export transport process. This assumption is supported by the previous results since *pdha* and *pdhb* expression increased after treatment and, consequently, high production of pyruvate is expected. Furthermore, *ldha* and *ldhb* expression levels increased after TAZ translocation to the nucleus, and lactate dehydrogenase is responsible for the reversible interconversion between pyruvate and lactate; accordingly, it is possible that the lactate present in the tissue is being converted into pyruvate. This hypothetical pyruvate accumulation could explain the increase in acetate levels but also the increase in succinate production.

Succinate extracellular levels are significantly higher for the 15 μM-treated explants comparing to controls. Succinate is an intermediate of the Krebs cycle or tricarboxylic acid (TCA) cycle and has a particularly important role in ATP generation in the mitochondria[161]. Succinate is the only direct connection between TCA and the mitochondrial respiratory chain; in the past few years, it has also been described as a potent signal transducer involved, for instance, in the immune signaling[162]. This pivotal TCA intermediary is formed by the conversion of succinyl-CoA, by succinyl-CoA synthetase, generating also ATP or GTP as final products[107]. The increase in the extracellular succinate levels is robust evidence that

chick embryonic lung metabolism is changing from its normal glycolytic-based metabolism towards a metabolic signature involving Krebs cycle and, consequently, oxidative phosphorylation.

The increase in the levels of acetate and succinate was detected in the extracellular medium which means that both metabolites need to be, somehow, transported out of the tissue. Eventually, MCT8 may be involved in acetate export, however, this assumption lacks supportive literature and more experimental data.

## 5.5. Metabolome analysis

Embryonic chick lung metabolomic signature is still largely unknown. Unpublished data from our group revealed that the embryonic chicken lung shows a glycolytic preference with a shift to lactate production as pulmonary branching occurs *in vitro* and by analyzing the extracellular medium. To characterize the metabolite profile of lung tissue, a metabolomic approach was performed by $^{1}$H-NMR, focusing on certain metabolite families including amino acids (alanine, glutamate and glycine), nucleotides (adenosine, adenosine monophosphate, adenosine triphosphate and inosine monophosphate) and glycolysis and Krebs-associated metabolites (glucose, lactate, pyruvate and succinate). Additionally, other metabolites were also quantified, namely, formate, taurine, O-phosphocholine, creatine, and acetate.

Regarding the amino acids, glutamate was the more abundant amino acid detected. Glutamate is one of the 20 canonical amino acids and is generally present in high levels in the tissues because: it is chemically stable; it is easily produced and removed metabolically by interconversion with α-ketoglutarate, a TCA intermediate; and, finally, it is negatively charged. The negative charge stabilizes the protein structure. Glutamate is classified as a non-essential amino acid and, for this reason, it must be synthesized in adequate quantities, *in vivo*[163]. Altogether, the presence of high quantities of glutamate in the embryonic lung tissue seems to be coherent with the literature.

Alanine is, also, a non-essential amino acid that is present in the embryonic lung. Alanine is synthesized via pyruvate, by transamination with glutamate. This process includes two different steps. First, α-ketoglutarate, ammonia and NADH are converted into glutamate, $NAD^{+}$ and water by the action of glutamate dehydrogenase. Next, the glutamate amino group is transferred to pyruvate, by an aminotransferase enzyme, leading to the regeneration of α-ketoglutarate and converting pyruvate to alanine[107].

Glycine is a non-essential amino acid obtained from dietary sources and from endogenous synthesis. It can be obtained from glucose, betaine (trimethylglycine), glyoxylate, likely from threonine and during the endogenous synthesis of L-carnitine. Glycine can be used in several metabolic pathways and can be used to synthesize other molecules like, for instance, serine by the action of serine hydroxymethyl transferase; N-methylglycine (sarcosine) by glycine methylation; and acyl-glycine derivatives, glutathione, heme group, collagen, and creatine[164].

Growing tissue needs to produce a high amount of proteins and other macromolecules in order to sustain the newly formed cells. The high amounts of amino acids present in the developing lung may be explained by the expected intense biosynthetic activity in this tissue.

Concerning nucleotides, it was possible to quantify adenosine, adenosine monophosphate (AMP), adenosine triphosphate (ATP) and inosine monophosphate (IMP). IMP is formed during the synthesis of purines by the deamination of adenosine monophosphate[107]. Adenosine is a nucleoside of adenine in glycosidic association with the sugar ribose. It serves as a precursor and metabolite of adenine nucleotides and can act as an extracellular signaling molecule[165]. AMP is formed in a series of reactions involving IMP, aspartate, and fumarate. ATP is responsible for providing energy to cellular processes and, when consumed, it is converted into adenosine diphosphate (ADP) or AMP. Taken together, these results point to an intense biosynthetic activity for generating nucleic acids and to an ATP pool necessary to cope with the high energetic requirements of the tissue. Both nucleic acids and ATP are absolutely necessary for proper organ development.

The energetic needs of the developing lung are mostly fulfilled by glucose catabolism, particularly, a glycolytic metabolism directed to lactate production. Interestingly, glucose was not detected in the tissue suggesting a high glycolytic rate and a rapid turnover. On the other hand, our results have showed that the amount of lactate present in the pulmonary tissue is much higher than pyruvate and succinate. These findings are in agreement with the unpublished data from our group that reported an increase in lactate production as branching morphogenesis proceeds. In the adult lung, a high percentage of the consumed glucose is converted into lactate and metabolic intermediaries that fuel biosynthetic pathways like the pentose phosphate pathway[166]. Overall, lactate-dependent metabolism appears to be necessary to fulfill the metabolic requirements of both adult and embryonic lung. Indirectly, these findings also corroborate our hypothesis that TM-treated lungs are going thru a metabolic rewiring towards TCA and oxidative phosphorylation (OXPHOS).

Although glycolysis presents an energetic yield of only two molecules of ATP/glucose, it supplies many important biosynthetic precursors for major macromolecules including carbohydrates, proteins, lipids, nucleic acids, and reducing power like the NADH from the pentose phosphate pathway[166,167]. All these intermediaries are crucial for proliferating cells and growing tissues during organogenesis.

Besides amino acids, nucleotides and Krebs cycle/glycolytic intermediaries, other metabolites were also quantified. Formate was recently shown as a potential biomarker for cancer diagnosis. In lung cancer, for instance, patients present lower serum levels of formate but in colorectal cancer, the amount of formate present is very high. Additionally, several studies have shown that increased levels of serum formate are associated with tumors exhibiting a high oxidative metabolism[168]. The low levels of formate in the embryonic lung match the glycolytic-lactate based metabolism described for the normal chick embryonic lung.

Taurine conjugation with mitochondrial tRNA for leucine and lysine promotes effective mitochondrial protein translation; it is, therefore, crucial for mitochondrial function especially for the expression of proteins in the electron transport chain, namely the complexes 1, 3 and 4 and ATP synthase[169]. The elevated presence of taurine in the lung may respond to the necessity of generating the proper cellular energetic machinery providing cells with mechanisms of obtaining high amounts of energy.

O-phosphocholine is an intermediate in the synthesis of phosphatidylcholine. Choline is phosphorylated to phosphocholine which is then is converted into phosphatidylcholine[170]. Phosphatidylcholine is a phospholipid and a major component of biological membranes. Taking into account that proliferative/developing tissues need high amounts of membrane components, the presence of o-phosphocholine is expected.

Creatine is an amine synthesized by the liver and kidneys using arginine, glycine, and methionine[171]. When phosphorylated, creatine is converted into phosphocreatine, which has a high energetic phosphate bond that can be cleaved and used for ATP reconstitution from ADP[107]. The presence of creatine in the developing lung may be explained by the need for developing tissues to obtaining fast energy in the form of ATP. So, creatine in this context can be seen as a precursor of ATP regeneration. Acetate can be produced from acetyl-CoA; since pyruvate was also detected in the tissue its presence is justifiable.

This work brings new insights concerning the metabolic regulation during lung branching morphogenesis. TAZ is involved in the mechanisms underlying lung morphogenesis since TAZ manipulation caused a mild increase in branching. However, at the molecular level, we observed profound changes in the expression levels of several transporters and enzymes involved in glucose catabolism, which is suggested to be the main energy source for developing tissues. In figure 17, a schematic representation of the TAZ-induced metabolism associated with chick lung branching is represented.

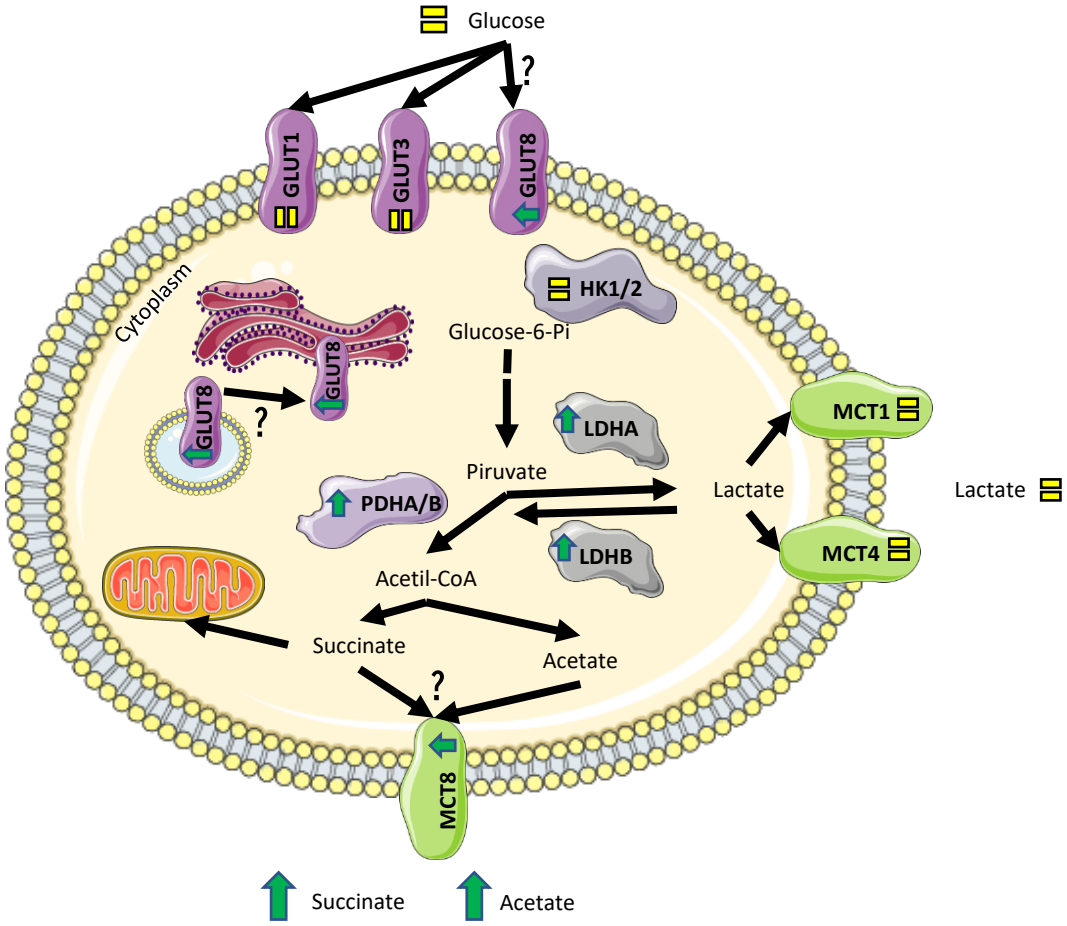


**Figure 17. Schematic representation of the TAZ-induced metabolism associated with chick lung branching.** The metabolites detected in the extracellular medium can either be consumed (glucose) or produced (lactate, succinate and acetate). The expression levels of glucose catabolism-related genes either transporters (GLUTs and MCTs) and enzymes (HK, PDH and LDH) were evaluated. Symbols refer to: (=) constant, (↑) increase and (?) hypothetical route.

The increased expression of *glut8*, *mct8*, *pdha*, *pdhb*, *ldha*, and *ldhb* points to a potential metabolic rewiring in the developmental chick lung. Furthermore, the metabolite profile was evidently altered; an increase in succinate (Krebs cycle) and acetate (synthesized from acetyl-CoA) was detected although glucose and lactate levels remained unchanged. The analysis of lung metabolome revealed that lactate is present in higher quantities than pyruvate; amino acids, nucleotides and other metabolites related to the biosynthetic activity during development were also identified.

To conclude, TAZ activity modulates branching and lung metabolism and these findings may help to unravel new therapeutic approaches to be applied in lung developmental disorders such as pulmonary hypoplasia.

# 6. Conclusions and Future Perspectives

Hippo signaling pathway is known to be involved in the regulation of cell growth, proliferation, survival, and organ-size control. Over the years, Hippo and other signaling pathways were deeply dissected in several morphogenesis-related processes in many organs, including the lung. However, the interplay between Hippo and developmental lung metabolism has not been described so far.

In this study, we described the role of TAZ in lung branching morphogenesis metabolism. TAZ manipulation elicited extensive metabolic alterations and promoted a shift from glucose-lactate based metabolism towards a more oxidative metabolism (TCA-dependent). The alterations in the lung metabolic signature were accompanied by changes in the expression levels of key glucose catabolism-related transporters and enzymes. Briefly, *glut8* may be facilitating the transport of sugars or sugar-derivatives in or out of intracellular organelles, thus contributing to biosynthetic events; moreover, it may be exporting, for instance, acetate or succinate. *pdh* and *ldh* may be contributing to pyruvate accumulation and, consequently, to a metabolic shift from glycolysis into the Krebs cycle and oxidative phosphorylation represented by acetate and succinate accumulation. Finally, the embryonic chick lung metabolome analysis revealed that lung tissue displays high levels of lactate when compared with succinate and acetate. The basal metabolite profile validates the changes observed due to TAZ manipulation that point to a metabolic rewiring towards the Krebs cycle and oxidative phosphorylation.

Further studies are needed to confirm some of the proposed hypothesis, namely, metabolome analysis of TAZ-stimulated explants to complete tissue metabolic profile and characterization of LDH and PDH protein expression levels. On the other hand, it would be interesting to unravel the underlying mechanism leading to TAZ-induced branching by characterizing its specific gene expression program and determine if it has impact in both proliferation and differentiation. By fully dissecting the mechanisms controlling lung growth through metabolic pathways, we hope to unravel new therapeutic strategies that might improve the treatment of lung growth disorders characterized by a reduction in lung size, as for instance, fetal pulmonary hypoplasia.

# 7. References


1. Morrisey, E. E. & Hogan, B. L. M. Preparing for the First Breath: Genetic and Cellular Mechanisms in Lung Development. Dev. Cell 18, 8–23 (2010).

2. Mullassery, D. & Smith, N. P. Lung development. Semin. Pediatr. Surg. 24, 152–155 (2015).

3. Herriges, M. & Morrisey, E. E. Lung development: orchestrating the generation and regeneration of a complex organ. Development 141, 502–513 (2014).

4. Lin, K. C. et al. Regulation of Hippo pathway transcription factor TEAD by p38 MAPK-induced cytoplasmic translocation. Nat. Cell Biol. 19, 996–1002 (2017).

5. Potente, M. & Carmeliet, P. The Link Between Angiogenesis and Endothelial Metabolism. Annu. Rev. Physiol. 79, 43–66 (2016).

6. Kleinstreuer, C., Zhang, Z. & Donohue, J. F. Targeted Drug-Aerosol Delivery in the Human Respiratory System. Annu. Rev. Biomed. Eng. 10, 195–220 (2008).

7. Arigliani, M., Spinelli, A. M., Liguoro, I. & Cogo, P. Nutrition and lung growth. Nutrients 10, 919 (2018).

8. Nikolić, M. Z., Sun, D. & Rawlins, E. L. Human lung development: recent progress and new challenges. Development 145, dev163485 (2018).

9. Chanda, D. et al. Developmental pathways in the pathogenesis of lung fibrosis. Mol. Aspects Med. 65, 56–69 (2019).

10. Gkatzis, K., Taghizadeh, S., Huh, D., Stainier, D. Y. R. & Bellusci, S. Use of three-dimensional organoids and lung-on-a-chip methods to study lung development, regeneration and disease. Eur. Respir. J. 52, 1800876 (2018).

11. Zhou, Y. et al. Extracellular matrix in lung development, homeostasis and disease. Matrix Biol. 73, 77–104 (2018).

12. Saito, A. & Nagase, T. Hippo and TGF-β interplay in the lung field. Am. J. Physiol. - Lung Cell. Mol. Physiol. L756–L767 (2015).

13. Fernandes-Silva, H., Correia-Pinto, J. & Moura, R. S. Canonical Sonic Hedgehog Signaling in Early Lung Development. J. Dev. Biol. 5, 3 (2017).

14. Hussain, M. et al. Wnt/β-catenin signaling links embryonic lung development and asthmatic airway remodeling. Biochim. Biophys. Acta - Mol. Basis Dis. 1863, 3226–3242 (2017).

15. Ning, J., Zhao, Y., Ye, Y. & Yu, J. Opposing roles and potential antagonistic mechanism between TGF-β and BMP pathways: Implications for cancer progression. EBioMedicine 41, 702–710 (2019).

16. Danopoulos, S., Shiosaki, J. & Al Alam, D. FGF Signaling in Lung Development and Disease: Human Versus Mouse. Front. Genet. 10, 170 (2019).

17. Nolte, C., De Kumar, B. & Krumlauf, R. Hox genes: Downstream "effectors" of retinoic acid signaling in vertebrate embryogenesis . Genesis e23306 (2019).

18. Yeung, B., Yu, J. & Yang, X. Roles of the Hippo pathway in lung development and tumorigenesis. Int. J. Cancer 138, 533–539 (2016).

19. Yang, J. & Chen, J. Developmental programs of lung epithelial progenitors: A balanced progenitor model. Wiley Interdiscip. Rev. Dev. Biol. 3, 331–347 (2014).

20. Schittny, J. C. Development of the lung. Cell Tissue Res. 367, 427–444 (2017).

21. Maina, J. N. Development, structure, and function of a novel respiratory organ, the lung-air sac system of birds: To go where no other vertebrate has gone. Biol. Rev. Camb. Philos. Soc. 81, 545–579 (2006).

22. Makanya, A. N. Membrane mediated development of the vertebrate blood-gas-barrier. Birth Defects Res. Part C - Embryo Today Rev. 108, 85–97 (2016).

23. Moura, R. S., Coutinho-Borges, J. P., Pacheco, A. P., daMota, P. O. & Correia-Pinto, J. FGF signaling pathway in the developing chick lung: Expression and inhibition studies. PLoS One 6, e17660 (2011).

24. Moura, R. S., Carvalho-Correia, E., DaMota, P. & Correia-Pinto, J. Canonical Wnt signaling activity in early stages of chick lung development. PLoS One 9, e112388 (2014).

25. Moura, R. S., Vaz-Cunha, P., Silva-Gonçalves, C. & Correia-Pinto, J. Characterization of miRNA processing machinery in the embryonic chick lung. Cell Tissue Res. 362, 569–575 (2015).

26. Moura, R. S., Silva-Gonçalves, C., Vaz-Cunha, P. & Correia-Pinto, J. Expression analysis of Shh signaling members in early stages of chick lung development. Histochem. Cell Biol. 146, 457–466 (2016).

27. Fernandes-Silva, H. et al. Retinoic acid regulates avian lung branching through a molecular network. Cell. Mol. Life Sci. 74, 4599–4619 (2017).

28. Deng, X. & Fang, L. VGLL4 is a transcriptional cofactor acting as a novel tumor suppressor via interacting with TEADs. Am J Cancer Res 8, 932–943 (2018).

29. Misra, J. R. & Irvine, K. D. The Hippo Signaling Network and Its Biological Functions. Annu. Rev. Genet. 52, 65–87 (2018).

30. Sharif, G. M. & Wellstein, A. Cell density regulates cancer metastasis via the Hippo pathway. Futur. Oncol. 11, 3253–3260 (2015).

31. Sun, Z. et al. FoxO6 regulates Hippo signaling and growth of the craniofacial complex. PLoS Genetics 14, e1007675 (2018).

32. Heallen, T. et al. Hippo pathway inhibits wnt signalling to restrain CM prolifeartion and hear size. Science 332, 458–461 (2011).

33. Lin, C., Yao, E., Chuang, P.T. A conserved MST1/2-YAP axis mediates Hippo signaling during lung growth HHS Public Access Author manuscript. Dev Biol 403, 101–113 (2015).

34. Mahoney, J. E., Mori, M., Szymaniak, A. D., Varelas, X. & Cardoso, W. V. The Hippo Pathway Effector Yap Controls Patterning and Differentiation of Airway Epithelial Progenitors. Dev. Cell 30, 137–150 (2014).

35. Zhao, R. et al. Yap Tunes Airway Epithelial Size and Architecture by Regulating the Identity, Maintenance, and Self-Renewal of Stem Cells. Dev. Cell 30, 151–165 (2014).

36. Lange, A. W. et al. Hippo/Yap signaling controls epithelial progenitor cell proliferation and differentiation in the embryonic and adult lung. J. Mol. Cell Biol. 7, 35–47 (2015).

37. Han, H. et al. Regulation of the Hippo Pathway by Phosphatidic Acid-Mediated Lipid-Protein Interaction. Mol. Cell 72, 328–340.e8 (2018).

38. Lin, C. et al. YAP is essential for mechanical force production and epithelial cell proliferation during lung branching morphogenesis. Elife 6, e21130 (2017).

39. Yin, F. et al. Spatial organization of hippo signaling at the plasma membrane mediated by the tumor suppressor merlin/NF2. Cell 154, 1342–1355 (2013).

40. Yi, C. et al. The p130 isoform of angiomotin is required for yap-mediated hepatic epithelial cell proliferation and tumorigenesis. Sci. Signal. 6, ra77 (2013).

41. Zhang, L. et al. NDR functions as a physiological YAP1 kinase in the intestinal epithelium. Curr. Biol. 25, 296–305 (2015).

42. Li, P. et al. αE-catenin inhibits a Src–YAP1 oncogenic module that couples tyrosine kinases and the effector of hippo signaling pathway. Genes Dev. 30, 798–811 (2016).

43. Mo, J. S. et al. Cellular energy stress induces AMPK-mediated regulation of YAP and the Hippo pathway. Nat. Cell Biol. 17, 500–510 (2015).

44. Panciera, T., Azzolin, L., Cordenonsi, M. & Piccolo, S. Mechanobiology of YAP and TAZ in physiology and disease. Nat. Rev. Mol. Cell Biol. 18, 758–770 (2017).

45. Totaro, A., Panciera, T. & Piccolo, S. YAP/TAZ upstream signals and downstream responses. Nat. Cell Biol. 20, 888–899 (2018).

46. Vogel, V. & Sheetz, M. Local force and geometry sensing regulate cell functions. Nat. Rev. Mol. Cell Biol. 7, 265–275 (2006).

47. Varelas, X. et al. The Hippo Pathway Regulates Wnt/β-Catenin Signaling. Dev. Cell 18, 579–591 (2010).

48. Hong, J. et al. TAZ, a Transcriptional Modulator of Mesenchymal Stem Cell Differentiation. Science 309, 1074–1078 (2005).

49. Zhang, W. et al. VGLL4 functions as a new tumor suppressor in lung cancer by negatively regulating the YAP-TEAD transcriptional complex. Cell Res. 24, 331–343 (2014).

50. Varelas, X. The Hippo pathway effectors TAZ and YAP in development, homeostasis and disease. Development 141, 1614–1626 (2014).

51. Liang, N. et al. Regulation of YAP by mTOR and autophagy reveals a therapeutic target of tuberous sclerosis complex. J. Exp. Med. 211, 2249–2263 (2014).

52. Huang, J., Wu, S., Barrera, J., Matthews, K. & Pan, D. The Hippo signaling pathway coordinately regulates cell proliferation and apoptosis by inactivating Yorkie, the Drosophila homolog of YAP. Cell 122, 421–434 (2005).

53. Zhao, B. et al. Inactivation of YAP oncoprotein by the Hippo pathway is involved in cell contact inhibition and tissue growth control. Genes Dev. 21, 2747–2761 (2007).

54. Dong, J. et al. Elucidation of a Universal Size-Control Mechanism in Drosophila and Mammals. Cell 130, 1120–1133 (2007).

55. Reginensi, A. et al. Yap and Cdc42-Dependent Nephrogenesis and Morphogenesis during Mouse Kidney Development. PLoS Genet. 9, (2013).

56. Nishioka, N. et al. The Hippo Signaling Pathway Components Lats and Yap Pattern Tead4 Activity to Distinguish Mouse Trophectoderm from Inner Cell Mass. Dev. Cell 16, 398–410 (2009).

57. Hirate, Y. et al. Polarity-dependent distribution of angiomotin localizes hippo signaling in preimplantation embryos. Curr. Biol. 23, 1181–1194 (2013).

58. Maître, J. L. et al. Asymmetric division of contractile domains couples cell positioning and fate specification. Nature 536, 344–348 (2016).

59. Mo, J. S., Park, H. W. & Guan, K.L. The Hippo signaling pathway in stem cell biology and cancer. EMBO Rep. 1–15 (2014). doi:10.15252/embr.201438638

60. Lian, I. et al. The role of YAP transcription coactivator in regulating stem cell self-renewal and differentiation. Genes Dev. 24, 1106–1118 (2010).

61. Panciera, T. et al. Induction of Expandable Tissue-Specific Stem/Progenitor Cells through Transient Expression of YAP/TAZ. Cell Stem Cell 19, 725–737 (2016).

62. Wang, X. et al. YAP/TAZ Orchestrate VEGF Signaling during Developmental Angiogenesis. Dev. Cell 42, 462–478.e7 (2017).

63. Feng, X. et al. Thromboxane A2 activates YAP/TAZ protein to induce vascular smooth muscle cell proliferation and migration. J. Biol. Chem. 291, 18947–18958 (2016).

64. Wang, K. C. et al. Flow-dependent YAP/TAZ activities regulate endothelial phenotypes and atherosclerosis. Proc. Natl. Acad. Sci. 113, 11525–11530 (2016).

65. Moroishi, T. et al. The Hippo Pathway Kinases LATS1/2 Suppress Cancer Immunity. Cell 167, 1525–1539.e17 (2016).

66. Yu, F. X., Zhao, B. & Guan, K. L. Hippo Pathway in Organ Size Control, Tissue Homeostasis, and Cancer. Cell 163, 811–828 (2015).

67. Lin, Z. & Pu, W. T. Harnessing Hippo in the heart: Hippo/Yap signaling and applications to heart regeneration and rejuvenation. Stem Cell Research 13, (2014).

68. Martin, K. et al. PAK proteins and YAP-1 signalling downstream of integrin beta-1 in myofibroblasts promote liver fibrosis. Nat. Commun. 7, 12502 (2016).

69. Zanconato, F., Cordenonsi, M. & Piccolo, S. YAP/TAZ at the Roots of Cancer. Cancer Cell 29, 783–803 (2016).

70. Yu, F. X. et al. Regulation of the Hippo-YAP pathway by G-protein-coupled receptor signaling. Cell 150, 780–791 (2012).

71. Meng, Z., Moroishi, T. & Guan, K. L. Mechanisms of Hippo pathway regulation. Genes Dev. 30, 1–17 (2016).

72. Santinon, G., Pocaterra, A. & Dupont, S. Control of YAP/TAZ Activity by Metabolic and Nutrient-Sensing Pathways. Trends Cell Biol. 26, 289–299 (2016).

73. Feng, X. et al. Hippo-independent activation of YAP by the GNAQ uveal melanoma oncogene through a Trio-regulated Rho GTPase Signaling Circuitry. Cancer Cell 25, 831–845 (2014).

74. Peng, C. et al. Regulation of the Hippo-YAP Pathway by Glucose Sensor O-GlcNAcylation. Mol. Cell 68, 591–604.e5 (2017).

75. Beyer, T. A. et al. Switch enhancers interpret TGF-β and hippo signaling to control cell fate in human embryonic stem cells. Cell Rep. 5, 1611–1624 (2013).

76. Manderfield, L. J. et al. Hippo signaling is required for Notch-dependent smooth muscle differentiation of neural crest. Development 142, 2962–2971 (2015).

77. Hubaud, A. & Pourquié, O. Signalling dynamics in vertebrate segmentation. Nat. Rev. Mol. Cell Biol. 15, 709–721 (2014).

78. Park, D. Y. et al. YAP/TAZ regulates sprouting angiogenesis and vascular barrier maturation. J. Clin. Invest. 127, 3441–3461 (2017).

79. Wang, W. et al. AMPK modulates Hippo pathway activity to regulate energy homeostasis. Nat. Cell Biol. 17, 490–499 (2015).

80. Straßburger, K., Tiebe, M., Pinna, F., Breuhahn, K. & Teleman, A. A. Insulin/IGF signaling drives cell proliferation in part via Yorkie/YAP. Dev. Biol. 367, 187–196 (2012).

81. deRan, M. et al. Energy stress regulates Hippo-YAP signaling involving AMPK-mediated regulation of angiomotin-like 1 protein. Cell Rep. 9, 495–503 (2014).

82. Zhang, X. et al. The essential role of YAP O-GlcNAcylation in high-glucose-stimulated liver tumorigenesis. Nat. Commun. 8, 15280 (2017).

83. Enzo, E. et al. Aerobic glycolysis tunes YAP/TAZ transcriptional activity. EMBO J. 34, 1349–1370 (2015).

84. Artinian, N. et al. Phosphorylation of the Hippo pathway component AMOTL2 by the mTORC2 kinase promotes YAP signaling, resulting in enhanced glioblastoma growth and invasiveness. J. Biol. Chem. 290, 19387–19401 (2015).

85. Sciarretta, S. et al. MTORC2 regulates cardiac response to stress by inhibiting MST1. Cell Rep. 11, 125–136 (2015).

86. Hu, J. K. H. et al. An FAK-YAP-mTOR Signaling Axis Regulates Stem Cell-Based Tissue Renewal in Mice. Cell Stem Cell 21, 91–106.e6 (2017).

87. Wang, L. et al. GCN5L1 modulates cross-talk between mitochondria and cell signaling to regulate FoxO1 stability and gluconeogenesis. Nat. Commun. 8, 523 (2017).

88. Singh, S., Simpson, R. L. & Bennett, R. G. Relaxin activates peroxisome proliferator-activated receptor γ (PPAR γ) through a pathway involving PPAR γ coactivator 1α (PGC1α). J. Biol. Chem. 290, 950–959 (2015).

89. Yu, F. X. et al. Protein kinase A activates the Hippo pathway to modulate cell proliferation and differentiation. Genes Dev. 27, 1223–1232 (2013).

90. Hu, Y. et al. YAP suppresses gluconeogenic gene expression through PGC1α. Hepatology 66, 2029–2041 (2017).

91. Sorrentino, G. et al. Metabolic control of YAP and TAZ by the mevalonate pathway. Nat. Cell Biol. 16, 357–366 (2014).

92. Wang, Z. et al. Interplay of mevalonate and Hippo pathways regulates RHAMM transcription via YAP to modulate breast cancer cell motility. Proc. Natl. Acad. Sci. 111, E89–E98 (2014).

93. Deng, Y., Matsui, Y., Pan, W., Li, Q. & Lai, Z. C. Yap1 plays a protective role in suppressing free fatty acid-induced apoptosis and promoting beta-cell survival. Protein Cell 7, 362–372 (2016).

94. Chan, P. et al. Autopalmitoylation of TEAD proteins regulates transcriptional output of the Hippo pathway. Nat. Chem. Biol. 12, 282–289 (2016).

95. Li, T. & Le, A. Glutamine Metabolism in Cancer. in (ed. Anne Le) 1063, 13–32 (Springer International Publishing, 2018).

96. Cluntun, A. A., Lukey, M. J., Cerione, R. A. & Locasale, J. W. Glutamine Metabolism in Cancer: Understanding the Heterogeneity. Trends in Cancer 3, 169–180 (2017).

97. Cox, A. G. et al. Yap reprograms glutamine metabolism to increase nucleotide biosynthesis and enable liver growth. Nat. Cell Biol. 18, 886–896 (2016).

98. Bertero, T. et al. Vascular stiffness mechanoactivates YAP/ TAZ-dependent glutaminolysis to drive pulmonary hypertension. J. Clin. Invest. 126, 3313–3335 (2016).

99. Morin-Kensicki, E. M. et al. Defects in Yolk Sac Vasculogenesis, Chorioallantoic Fusion, and Embryonic Axis Elongation in Mice with Targeted Disruption of Yap65. Mol. Cell. Biol. 26, 77–87 (2005).

100. Makita, R. et al. Multiple renal cysts, urinary concentration defects, and pulmonary emphysematous changes in mice lacking TAZ. Am. J. Physiol. Physiol. 294, F542–F553 (2008).

101. Mitani, A. et al. Transcriptional coactivator with PDZ-binding motif is essential for normal alveolarization in mice. Am. J. Respir. Crit. Care Med. 180, 326–338 (2009).

102. Danopoulos, S. et al. Human lung branching morphogenesis is orchestrated by the spatiotemporal distribution of ACTA2, SOX2, and SOX9. Am. J. Physiol. Cell. Mol. Physiol. 314, L144–L149 (2017).

103. Mao, Y. et al. Characterization of a Dchs1 mutant mouse reveals requirements for Dchs1-Fat4 signaling during mammalian development. Development 138, 947–957 (2011).

104. Chung, C. et al. Hippo-Foxa2 signaling pathway plays a role in peripheral lung maturation and surfactant homeostasis. Proc. Natl. Acad. Sci. 110, 7732–7737 (2013).

105. Warburg, O. On the origin of cancer cells. Science 123, 309–314 (1956).

106. Akram, M. Mini-review on glycolysis and cancer. J. Cancer Educ. 28, 454–457 (2013).

107. Cox, M. M. & Nelson, D. L. Lehninger's Principles of Biochemistry (2008).

108. Agathocleous, M. & Harris, W. A. Metabolism in physiological cell proliferation and differentiation. Trends Cell Biol. 23, 484–492 (2013).

109. Bulusu, V. et al. Spatiotemporal Analysis of a Glycolytic Activity Gradient Linked to Mouse Embryo Mesoderm Development. Dev. Cell 40, 331–341.e4 (2017).

110. Oginuma, M. et al. A Gradient of Glycolytic Activity Coordinates FGF and Wnt Signaling during Elongation of the Body Axis in Amniote Embryos. Dev. Cell 40, 342–353.e10 (2017).

111. Carraro, G., del Moral, P.M. & Warburton, D. Mouse Embryonic Lung Culture, A System to Evaluate the Molecular Mechanisms of Branching. J. Vis. Exp. 40, e2035 (2010).

112. Moral, P. & Warburton, D. Mouse Cell Culture. 633, 71–79 (2010).

113. Bradford, M. M. A rapid and sensitive method for the quantitation of microgram quantities of protein utilizing the principle of protein-dye binding. Anal. Biochem. 72, 248–254 (1976).

114. Ku, H. K. et al. Interpretation of protein quantitation using the Bradford assay: Comparison with two calculation models. Anal. Biochem. 434, 178–180 (2013).

115. Yang, P.-C. & Mahmood, T. Western blot: Technique, theory, and trouble shooting. N. Am. J. Med. Sci. 4, 429 (2012).

116. Taylor, S. C. & Posch, A. The Design of a Quantitative Western Blot Experiment. Biomed Res. Int. 2014, 361590 (2014).

117. Nowakowski, A. B., Wobig, W. J. & Petering, D. H. Native SDS-PAGE: High resolution electrophoretic separation of proteins with retention of native properties including bound metal ions. Metallomics 6, 1068–1078 (2014).

118. Brunelle, J. L. & Green, R. One-dimensional SDS-polyacrylamide gel electrophoresis (1D SDS-PAGE). Methods in Enzymology 541, (Elsevier Inc., 2014).

119. Luk, P. P. et al. Clinical Utility of In Situ Hybridization Assays in Head and Neck Neoplasms. Head Neck Pathol. 1-18 (2018).

120. Volpi, C. C. et al. Bright-field in situ hybridization detects gene alterations and viral infections useful for personalized management of cancer patients. Expert Rev. Mol. Diagn. 18, 259–277 (2018).

121. Holleville, N., Matéos, S., Bontoux, M., Bollerot, K. & Monsoro-Burq, A. H. Dlx5 drives Runx2 expression and osteogenic differentiation in developing cranial suture mesenchyme. Developmental Biology 304, 860–874 (2007).

122. Green, M. & Sambrook, J. Molecular Cloning, a laboratory manual. 1, (John Inglis, 2012).

123. Henrique, D. et al. Expression of a Delta homologue in prospective neurons in the chick. Nature 375, 787–790 (1995).

124. Klein, D. Quantification using real-time PCR technology: applications and limitations. Trends Mol. Med. 8, 257–60 (2002).

125. Pfaffl, M. W. A new mathematical model for relative quantification in real-time RT-PCR. Nucleic Acids Res. 29, e45 (2001).

126. Mussap, M., Zaffanello, M. & Fanos, V. Metabolomics: A challenge for detecting and monitoring inborn errors of metabolism. Biochim. Clin. 43, 14–23 (2019).

127. Gagnebin, Y., Boccard, J., Ponte, B. & Rudaz, S. Metabolomics in chronic kidney disease: Strategies for extended metabolome coverage. J. Pharm. Biomed. Anal. 161, 313–325 (2018).

128. Alves, M. G., Oliveira, P. F., Martins, F. O., Oliveira, P. J. & Carvalho, R. A. Gender-dependent metabolic remodeling during heart preservation in cardioplegic celsior and histidine buffer solution. J. Cardiovasc. Pharmacol. 59, 151–157 (2012).

129. Jang, E. J. et al. TM-25659 enhances osteogenic differentiation and suppresses adipogenic differentiation by modulating the transcriptional co-activator TAZ. Br. J. Pharmacol. 165, 1584–1594 (2012).

130. San Martin, I. A. et al. Impaired cell cycle regulation of the osteoblast-related heterodimeric transcription factor Runx2-Cbfβ in osteosarcoma cells. in Journal of Cellular Physiology 221, 560–571 (2009).

131. Zhu, Y. et al. Pharmacological activation of TAZ enhances osteogenic differentiation and bone formation of adipose-derived stem cells. Stem Cell Res. Ther. 9, 53 (2018).

132. Nishio, M. et al. The Hippo Signaling Pathway: A Candidate New Drug Target for Malignant Tumors. in Innovative Medicine (eds. Nakao, K., Minato, N. & Uemoto, S.) 79–94 (Springer, 2015).

133. Yuan, T., Volckaert, T., Chanda, D., Thannickal, V. J. & De Langhe, S. P. Fgf10 Signaling in Lung Development, Homeostasis, Disease, and Repair After Injury. Front. Genet. 9, 418 (2018).

134. Yin, Y. et al. An FGF-WNT gene regulatory network controls lung mesenchyme development. Dev. Biol. 319, 426–436 (2008).

135. Volckaert, T. et al. Fgf10-Hippo Epithelial-Mesenchymal Crosstalk Maintains and Recruits Lung Basal Stem Cells. Dev. Cell 43, 48–59.e5 (2017).

136. Maruyama, Z. et al. Runx2 determines bone maturity and turnover rate in postnatal bone development and is involved in bone loss in estrogen deficiency. Dev. Dyn. 236, 1876–1890 (2007).

137. Yoshida, C. A. et al. Runx2 and Runx3 are essential for chondrocyte maturation, and Runx2 regulates limb growth through induction of Indian hedgehog. Genes Dev. 18, 952–963 (2004).

138. Qin, X., Jiang, Q., Miyazaki, T. & Komori, T. Runx2 regulates cranial suture closure by inducing hedgehog, Fgf, Wnt and Pthlh signaling pathway gene expressions in suture mesenchymal cells. Hum. Mol. Genet. 28, 896–911 (2018).

139. Li, Y. Lin & Xiao, Z. Sheng. Advances in Runx2 regulation and its isoforms. Med. Hypotheses 68, 169–175 (2006).

140. Xiao, Z. S., Simpson, L. G. & Quarles, L. D. IRES-dependent translational control of Cbfa1/Runx2 expression. J. Cell. Biochem. 88, 493–505 (2003).

141. Herreño, A. M. et al. Role of RUNX2 transcription factor in epithelial mesenchymal transition in non-small cell lung cancer lung cancer: Epigenetic control of the RUNX2 P1 promoter. Tumor Biol. 41, 101042831985101 (2019).

142. Scheepers, A., Joost, H. G. & Schürmann, A. The glucose transporter families SGLT and GLUT: Molecular basis of normal and aberrant function. J. Parenter. Enter. Nutr. 28, 364–371 (2004).

143. Augustin, R., Riley, J. & Moley, K. H. GLUT8 contains [DE]XXXL[LI] sorting motif and localizes to a late endomosal/lysosomal compartment. Traffic 6, 1196–1212 (2005).

144. Piroli, G. G. et al. Peripheral glucose administration stimulates the translocation of GLUT8 glucose transporter to the endoplasmic reticulum in the rat hippocampus. J. Comp. Neurol. 452, 103–114 (2002).

145. Carayannopoulos, M. O. et al. GLUT8 is a glucose transporter responsible for insulin-stimulated glucose uptake in the blastocyst. Proc. Natl. Acad. Sci. 97, 7313–7318 (2002).

146. Schmidt, S., Joost, H.-G. & Schürmann, A. GLUT8, the enigmatic intracellular hexose transporter. Am. J. Physiol. Metab. 296, E614–E618 (2009).

147. Doege, H., Schürmann, A., Bahrenberg, G., Brauers, A. & Joost, H. G. GLUT8, a novel member of the sugar transport facilitator family with glucose transport activity. J. Biol. Chem. 275, 16275–16280 (2000).

148. Byers, M. S., Howard, C. & Wang, X. Avian and Mammalian Facilitative Glucose Transporters. Microarrays 6, 7 (2017).

149. Kono, T. et al. Characterisation of glucose transporter (GLUT) gene expression in broiler chickens. Br. Poult. Sci. 46, 510–515 (2005).

150. Seki, Y., Sato, K., Kono, T., Abe, H. & Akiba, Y. Broiler chickens (Ross strain) lack insulin-responsive glucose transporter GLUT4 and have GLUT8 cDNA. Gen. Comp. Endocrinol. 133, 80–87 (2003).

151. Halestrap, A. P. The monocarboxylate transporter family-Structure and functional characterization. IUBMB Life 64, 1–9 (2012).

152. Lafrenière, R. G., Carrel, L. & Willard, H. F. A novel transmembrane transporter encoded by the XPCT gene in xq13.2. Hum. Mol. Genet. 3, 1133–1139 (1994).

153. Friesema, E. C. H. et al. Identification of monocarboxylate transporter 8 as a specific thyroid hormone transporter. J. Biol. Chem. 278, 40128–40135 (2003).

154. Vancamp, P. & Darras, V. M. From zebrafish to human: A comparative approach to elucidate the role of the thyroid hormone transporter MCT8 during brain development. Gen. Comp. Endocrinol. 265, 219–229 (2018).

155. Stepien, B. K. & Huttner, W. B. Transport, Metabolism, and Function of Thyroid Hormones in the Developing Mammalian Brain. Front. Endocrinol. (Lausanne). 10, 209 (2019).

156. Park, S. et al. Role of the pyruvate dehydrogenase complex in metabolic remodeling: Differential pyruvate dehydrogenase complex functions in metabolism. Diabetes Metab. J. 42, 270–281 (2018).

157. Golias, T., Kery, M., Radenkovic, S. & Papandreou, I. Microenvironmental control of glucose metabolism in tumors by regulation of pyruvate dehydrogenase. Int. J. Cancer 144, 674–686 (2019).

158. Drent, M., Cobben, N. A. M., Henderson, R. F., Wouters, E. F. M. & Van Dieijen-Visser, M. Usefulness of lactate dehydrogenase and its isoenzymes as indicators of lung damage or inflammation. Eur. Respir. J. 9, 1736–1742 (1996).

159. Ding, J., Karp, J. E. & Emadi, A. Elevated lactate dehydrogenase (LDH) can be a marker of immune suppression in cancer: Interplay between hematologic and solid neoplastic clones and their microenvironments. Cancer Biomarkers 19, 353–363 (2017).

160. Feng, Y. et al. Lactate dehydrogenase A: A key player in carcinogenesis and potential target in cancer therapy. Cancer Med. 7, 6124–6136 (2018).

161. Porporato, P. E., Dhup, S., Dadhich, R. K., Copetti, T. & Sonveaux, P. Anticancer targets in the glycolytic metabolism of tumors: A comprehensive review. Front. Pharmacol. 2, 49 (2011).

162. Tielens, A. G. M., van Grinsven, K. W. A., Henze, K., van Hellemond, J. J. & Martin, W. Acetate formation in the energy metabolism of parasitic helminths and protists. Int. J. Parasitol. 40, 387–397 (2010).

163. Cho, E. H. Succinate as a regulator of hepatic stellate cells in liver fibrosis. Front. Endocrinol. (Lausanne). 9, 455 (2018).

164. Murphy, M. P. & O'Neill, L. A. J. Krebs Cycle Reimagined: The Emerging Roles of Succinate and Itaconate as Signal Transducers. Cell 174, 780–784 (2018).

165. Brosnan, J. T. & Brosnan, M. E. Glutamate: A truly functional amino acid. Amino Acids 45, 413–418 (2013).

166. Adeva-Andany, M. et al. Insulin resistance and glycine metabolism in humans. Amino Acids 50, 11–27 (2018).

167. Gorzalczany, Y. & Sagi-eisenberg, R. Role of Mast Cell-Derived Adenosine in Cancer. 20, 2603 (2019).

168. Tierney, D. F. Lung Metabolism and Biochemistry. Annu. Rev. Physiol. 36, 209–231 (2003).

169. Orang, A. V., Petersen, J., McKinnon, R. A. & Michael, M. Z. Micromanaging aerobic respiration and glycolysis in cancer cells. Mol. Metab. 23, 98–126 (2019).

170. Pietzke, M. et al. Stratification of cancer and diabetes based on circulating levels of formate and glucose. Cancer Metab. 7, 3 (2019).

171. Lambert, I. H., Kristensen, D. M., Holm, J. B. & Mortensen, O. H. Physiological role of taurine–from organism to organelle. Acta Physiol. (Oxf). 213, 191–212 (2015).

172. Jansen, S. M. et al. Biosynthesis of Phosphatidylcholine from a Phosphocholine Precursor Pool Derived from the Late Endosomal/Lysosomal Degradation of Sphingomyelin. J. Biol. Chem. 276, 18722–18727 (2001).

173. Almeida, F. M. et al. Creatine supplementation attenuates pulmonary and systemic effects of lung ischemia and reperfusion injury. J. Hear. Lung Transplant. 35, 242–250 (2016).

# 8. Appendix 1

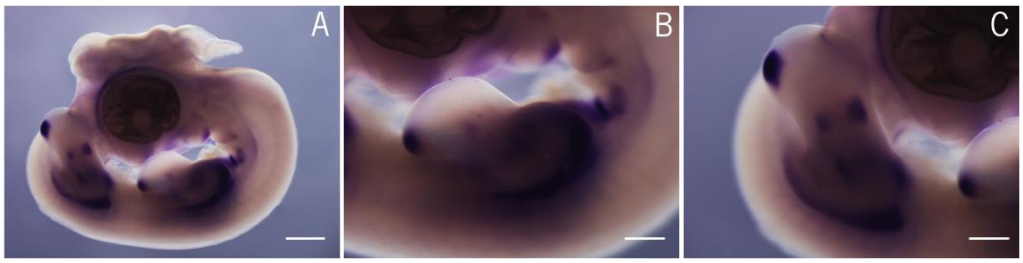


**Figure 18. Characterization of *runx2* expression by *in situ* hybridization in whole embryos.** (A) Representative examples of *in situ hybridization* for *runx2* of HH25 stage. (B) and (C) are magnifications of upper and lower limbs, respectively (n=4). Scale bar: (A), 1000 µm (B/C), 500 µm.

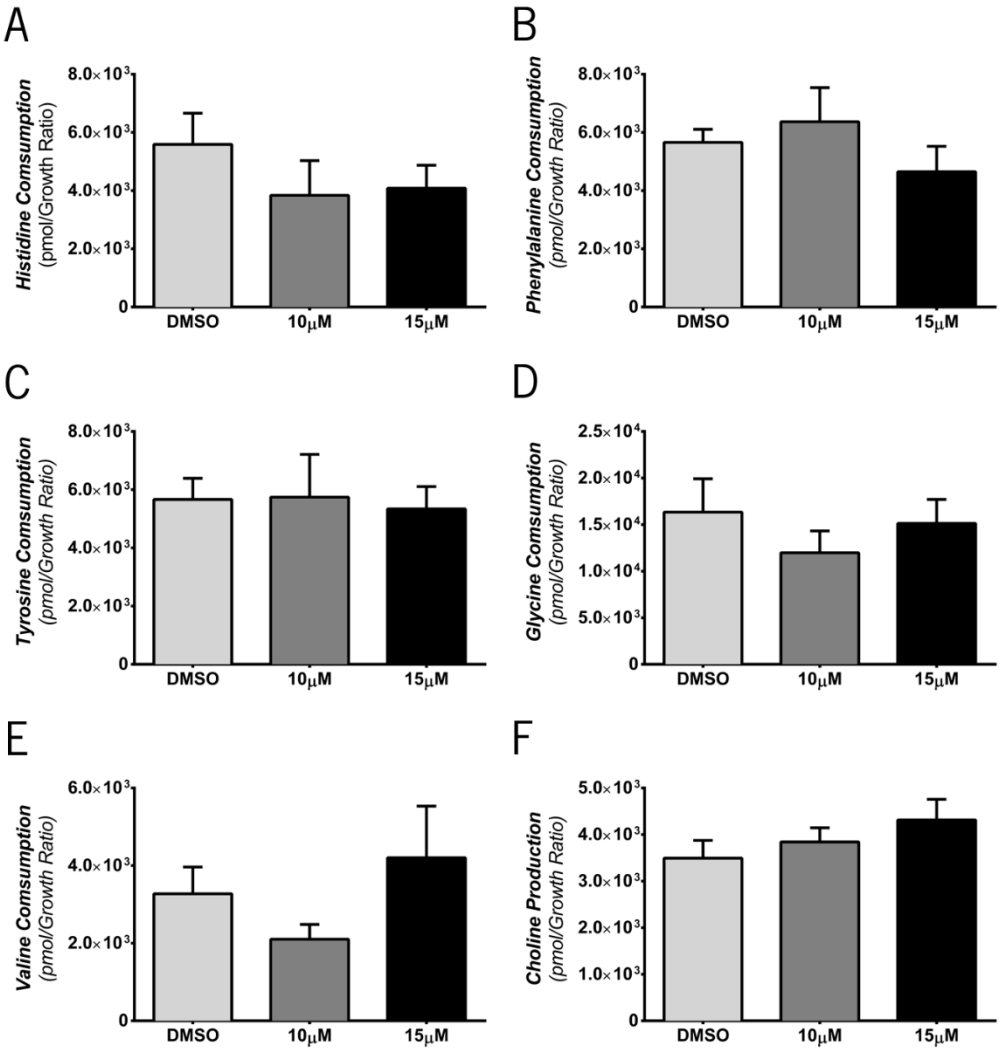


**Figure 19. Metabolite concentration after TAZ stimulation with TM-25659 for 48 hours.** Representation of histidine consumption (A), phenylalanine production (B), tyrosine consumption (C), glycine consumption (D), valine consumption (E) and choline production (F). Results are expressed as mean ± SEM (n≥6/condition).